Fall 2012

Modeling of the radial compressive properties of an aortic stent graft

Chaid Daniel Schwarz
University of Iowa

MODELING OF THE RADIAL COMPRESSIVE PROPERTIES OF AN AORTIC

STENT GRAFT

by

Chaid Daniel Schwarz

A thesis submitted in partial fulfillment
of the requirements for the Master of
Science degree in Biomedical Engineering
in the Graduate College of
The University of Iowa

December 2012

Thesis Supervisor: Professor Madhavan L. Raghavan

Graduate College
The University of Iowa
Iowa City, Iowa

CERTIFICATE OF APPROVAL

_____

MASTER'S THESIS

_____

This is to certify that the Master's thesis of

Chaid Daniel Schwarz

has been approved by the Examining Committee
for the thesis requirement for the Master of Science
degree in Biomedical Engineering at the December 2012 graduation.

Thesis Committee: _____
                  Madhavan L. Raghavan, Thesis Supervisor

                  _____
                  Nicole Grosland

                  _____
                  Jia Lu

                  _____
                  Edward Sander

                  _____
                  Sarah Vigmostad

ACKNOWLEDGMENTS

ABSTRACT

Abdominal aortic aneurysms are a focal dilation of the aorta which can be potentially life threatening if left untreated. Endovascular aneurysm repair (EVAR) is a noninvasive treatment that can reduce the mortality rate when compared to the standard open repair. Yet, EVAR is associated with other complications that can arise such as migration, endoleaks, or device related failures. These complications drive the need for reinterventions which have been shown to occur more frequently with EVAR than with open repair. The long term fixation and sealing characteristics of these devices is likely related to the nature of its apposition to the aortic wall. Currently there is little understanding of these mechanics and factors in how the device performs at the time of deployment. A computational model that reflects the compressive nature of an endovascular graft is beneficial in investigating these mechanics. The aims of the study are; 1) formulate an experimental methodology that captures the radial compressive nature of the stent graft, 2) develop a parameterized finite element model of the stent structure, and 3) compare the compressive behavior this model against the acquired experimental data.

A 2 mil polyethylene sleeve was used to transfer a compressive vacuum pressure from the sleeve onto 10 independent stent grafts. The loading-unloading pressure was cycled from 0 to -50 mmHg (complete collapse) over 5 minutes. A pressure transducer and optical micrometer were used to capture the vacuum pressure and diameter relationship. All ten grafts compressed in a similar elliptical shape configuration. Commercial software was leveraged to construct a parameterized model of the stent geometry. All crest and trough vertex locations of the sinusoidal stent structure were validated within 1 mm of a measured value. A dynamic quasi-static computational simulation was completed that included large deformations and contact between the sleeve and stent as well as self-contact in the sleeve. Our results show that the model is

representative of the experiments and can be used to interrogate how a stent graft will perform during certain stages of deployment and immediately after deployment with some caution in regard to the stated limitations.

TABLE OF CONTENTS

LIST OF TABLES

LIST OF FIGURES

vii

CHAPTER 1: INTRODUCTION

Abdominal Aortic Aneurysms

Aneurysms are a disease of the arterial pathways which deliver oxygenated blood from the heart to the organs and tissues throughout the body. By geometric definition aneurysms are a ballooning or dilatation of an arterial segment greater than 50% of its nominal diameter [14]. Juxtaposed to the elements that visually define an aneurysm is the complexity of what is occurring within the tissue. Though what causes an aneurysm is not clearly understood there are some factors that may lead to the weakening of the arterial wall such as smoking, high blood pressure, age and genetics [11,34]. Regardless of the cause, if an aneurysm manifests itself it can significantly increase the risk of arterial rupture depending on the state of the aneurysm. Abdominal aortic aneurysms (AAA) are the most common type of aneurysm and approximately 200,000 are diagnosed each year. Of these diagnoses roughly 15,000 are conditioned as life threatening if they were to rupture (http://www.vascularweb.org). Abdominal aortic aneurysms are commonly located just below the renal arteries (infrarenal) but above the point in which the descending aorta bifurcates into the two femoral arteries.

Typically two main factors along with patient history are accounted for in the decision to pursue treatment; aneurysm size and growth rate. It is suggested that a practitioner treat the aneurysm, depending on patient history and circumstances, if an aneurysm diameter is above the suggested threshold of 5.5 cm (4.0-4.5 cm for women) or if an aneurysm is followed to dilate more than 1 cm per year [3].

Treatment of AAAs

Treatments of AAAs utilize device implants that work to depressurize the aneurysm while creating a new blood pathway. Surgeons traditionally (yr. 1951-current) perform what is considered an open repair to treat patients with a high risk of rupture. In an open repair the surgeon will open the abdominal cavity, clamp the aorta just above and

below the aneurysm and then sew a fabric tube or graft made of polyethylene terephthalate (Dacron or PET) or polytetrafluoroethylene (PTFE) inside the aneurysm. Both the proximal and distal segments are stitched to healthy tissue as seen in Figure 1.
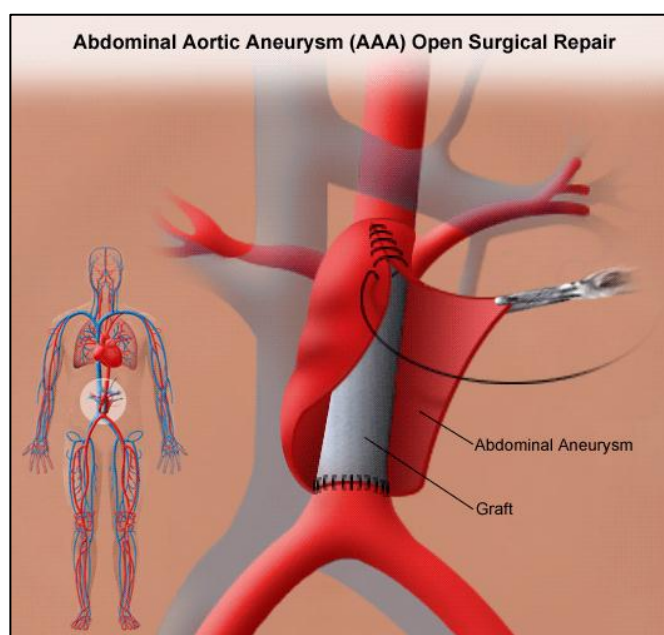
Figure 1: Open surgical repair procedure.

Source: Stanford Hospital and Clinics (www. Stanfordhospital.org). Available from: (http://stanfordhospital.org/clinicsmedServices/CO E/surgicalServices/vascularSurgery/patientEducati on/abdominalAorticAneurysmRepair.html)

This graft then acts as a synthetic vascular replacement reinforcing the diseased arterial tissue. Standard open repair is well documented to show its effectiveness and durability in treating AAAs [10,7,12] yet in some centers it has been shown to have rates of mortality of 5-10% [15,16,19] and major complications. Though open repair is the standard and still performed it may not be the best choice of procedures depending on a patient's age, condition and or medical history. Along with mortality open repair has possible

perioperative and post-operative complications including morbidities such as infection, excessive bleeding and prolonged reduced blood flow for the lower extremities (Rutherford). The last two decades have brought about new options in the treatment of AAA's.

Endovascular aneurysm repair (EVAR) is one such procedure (Figure 2).   The
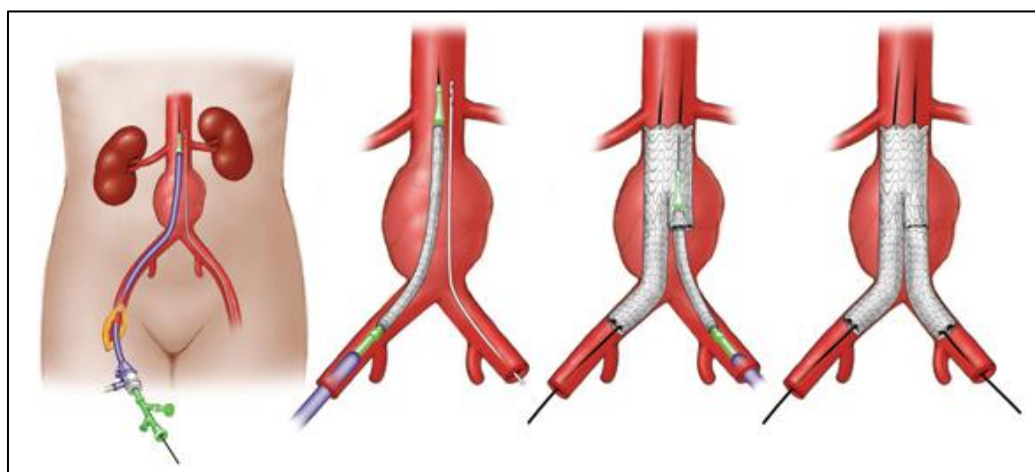
Figure 2: Endovascular aneurysm repair.

Source: Mayo Clinic (www.mayoclinic.org). Available from:
(http://www.mayoclinic.org/medicalprofs/enlargeimage5675.html)

first EVAR procedure was done by Parodi in 1990 [22]. This procedure and its noninvasive techniques have modernized the treatment of AAAs. As such, EVAR has become progressively accepted for patients who otherwise may not be suitable for open repair [1]. When undergoing an EVAR procedure an endovascular graft (EVG) or stent graft (SG) is crimped by concentric radial compression and placed into a flexible catheter. A small incision is made in a femoral artery where the catheter is inserted and guided up the artery until it reaches the abdominal aneurysm. The stent graft is then positioned where the proximal and distal ends would contact regions of healthy tissue. It is then deployed

into the lumen of the artery. For modular devices, a similar set of steps are done in the contralateral femoral artery. Here, a secondary endoprothesis leg is inserted connecting the main device body to the other descending femoral artery. Endovascular repair helps resolve some of the issues that plague open repair but it is not without its own clinical or mechanical complications as well. Generally all SG's are subject to potential problems such as device migration, poor apposition, endoleaks and possible mechanical device failures among others [15]. Migration is considered a distal movement or dislodgement of the SG greater than 1 cm [6]. Endoleaks are the persistence of blood flow outside the lumen of the endoluminal graft but within the aneurysm sac [6]. Endoleaks are subdivided into four categories. A type I endoleak is indicative of blood flow between the graft and artery where an insufficient seal has been made in the proximal or distal graft ends. Type II endoleaks are attributed to retrograde blood flow from collateral vessels. Type III endoleaks are regarded as blood flow between adjoining modular endovascular graft segments and flow through the graft due to material damage such as a cut or tear. It also describes the blood flow between attachment sites where the graft is attached to the stent body but has become damaged allowing blood flow outside the stent graft. Type IV endoleaks occur when blood is able to transport through the graft material wall due to the porosity of the graft with in the first 30 days. Considering these potential failures, patients undergoing EVAR must have proper proximal and distal graft attachment sites. The specific requirements may vary between practitioners but generally they look at the amount of calcifications and the morphology for low vascular angulation, proper aortic neck lengths, and artery diameters that are within a device sizing range [28].

<p style="text-align:center">EVAR Treatment Background</p>

Historically, the first decade of endovascular repair came with enthusiasm and the procedure had a strong outlook as the modern treatment for abdominal aortic aneurysms. EVAR was seen as the resolve to some of the perioperative and short term complications

and mortalities that beset open repair. But while the stent graft devices provided some resolution to the perioperative and <30 day morbidities of open repair, they also introduced a new set of complications and questions of their long term durability. Early (first decade) reports of SG failure modes such as migration, stent failures, fabric fatigue, late ruptures and a significant incidence of secondary procedures expressed caution in their use [1,13]. In 2004 Rutherford and Krupski [26] stated that essentially all trials at that time that had compared open repair versus EVAR showed that, despite complication rates averaging close to 15%, EVAR significantly reduced systemic complications compared with OPEN (primarily cardiac and pulmonary, but not renal), but EVAR resulted in more local vascular complications (eg, groin hematoma, femoral artery injury). In midterm (early 2000s) results Dattilo et al. [8] showed reintervention rates of 11% and mortality of 1.6% for a 18 month follow-up period of patients across 7 years yet it was concluded that EVAR had good results for most properly selected patients but noted that it may not be as durable as open based repair. A retrospective study of the 3 year Dutch Randomized Endovascular Aneurysm Management (DREAM) Trial Group from the Netherlands and Belgium concluded similar outcomes. This randomized study looked at a 30 day mortality and morbidity rates. Open repair maintained higher short term mortality 4.6% compared to EVAR with 1.2% while combined mortality and morbidities were 9.8% and 4.7% respectively [24]. Other studies such as the UK based Endovascular Aneurysm Repair (EVAR-1) trial (years 1999-2003) had similar morality results (4.6% open and 1.6% EVAR). Reinterventions rates were 5.8% for open versus 9.8% for EVAR showing that despite higher reintervention rates or complications EVAR significantly reduced short term open repair mortalities [20]. While the short term benefit could be seen the long term benefit ensuring the patient would remain free from aneurysm related mortality and morbidity after treatment was unknown of open repair versus EVAR. A study by Bruin et. al. [4] analyzed the results of the DREAM (years 2000-2003) study after a median of 6.4 years and showed the overall survival rates of 69.9% for open repair and 68.9% of

EVAR. It was also noted that significantly higher rates of reintervention were required after six years (18.1% for open vs. 29.6% for EVAR) which lead to a conclusion that "short term survival benefit of endovascular repair is achieved at the expense of long-term problems related to endograft durability." Here durability references the need for reintervention from graft related (endoleak, migration, graft failure, infection), wound related and systemic indications (type II endoleak, bleeding). Certainly practitioner patient selection criterion, available medical devices and procedure protocols have improved since this data was collected. In fact given the benefit of short term advantages yet long term challenges with EVAR, recent reports of the newer generation devices show a paradigm shift in medical procedure selection from the midterm (early 2000s) reports of cautioned use. EVAR selection in the late 1990s increased to ~60% then in the early 2000s was ~40% and by 2008 it had climbed to ~80% [1]. Similarly in a larger case study, Chadi et. al. [5] showed that the early (2001-2003) EVAR represented only ~30% of all treated cases. More recent years (2008-2010) showed a large increase in AAA treatment with endovascular grafts. In 2010, this resulted in 66% of cases being treated with EVG's out of a population of 1,942 patients. The reinvigorated use of stent grafts for treatment of AAA's certainly shows a renewed value in the newer devices to perform to exceptions better than or equal to open repair for selected patients. As mentioned by Albuquerque et al.[1], with newer and better devices some treatments may push the bounds of the SG based repair when difficult patient complications are adverse for open repair. Yet there are still the lingering questions as to the long term durability of even these newer devices. While the technical ability and improved short term benefits of newer EVAR may make this hopeful for patients it will only do so if the stent graft is durable enough to ensure the patient remains free from aneurysm related mortality and morbidities [27]. Though newer generation device designs are certain to focus on the issues that have been reported, current options undoubtedly have some challenges ahead.

Endovascular Graft Devices

Currently there are 8 endograft devices that are FDA approved for retail in the U.S.A., they are summarized in Table 1. The design and materials of stent grafts are

Table 1: Currently available EVG devices.

Company	Graft Name	FDA Approval	Stent Location	Stent Material
W.L.Gore	Excluder	November 2002	External	Nitinol
Cook Medical	Zenith Flex	June 2004	External	SS/Nitinol
Medtronic	AneuRX	September 1999	External	Nitinol
	Talent	April 2008	External	Nitinol
	Endurant II	June 2012	External	Cobalt Cr.
Endologix	Powerlink	October 2004	Internal	Cobalt Cr.
	AFX	June 2011	Internal	Cobalt Cr.
Trivascular	Ovation	October 2012	External	Nitinol

generally built upon similar underlying concepts, though the designs themselves are distinctly different. Generally it is considered that the radial forces are primarily carried by a wire that is typically a stainless steel, cobalt chromium metal or Nitinol alloy. The Nitinol is a superelastic memory shape alloy that has two temperature phase characteristics-martensite and austenite-which are temperature dependent. As a superelastic metal alloy material, it retains the ability to undergo large strain (~10%) and still be able to reshape back to its initial geometry when the stressing load is removed. The shape memory properties of Nitinol are defined by a thermal phase transformation based on the alloy composition and material processing. Typically for self-expanding stents the transformation temperature is ~30°C but this can be adjusted based on

composition and processing. As such for each degree that the transition temperature is below body temperature the loading unloading forces increase by approximately 4 N/mm [30].

For some devices, the wire geometry is sinusoidal and helically wrapped continuously around the graft. Other designs have sinusoidal wires but utilize individual wire segments spaced along the graft where each segment makes only one revolution around the graft. These two design formats are considered open celled stents. Finally, Endologix (Irvine, CA) and the Medtronic (Minneapolis, MN) AneuRX devices utilize a closed cell stent structure. Here a wire is in the shape of a diamond and is patterned around the graft circumference and then that is patterned in the axial direction.

The graft, which is fabric like in its behavior, is made of expanded polyterafluoroethylene (ePTFE), PTFE or PET (Dacron) and is primarily used as the conduit for the blood flow. It also must act as the sealing agent in the proximal, distal and at the modular contralateral leg interface in order to keep the aneurysm depressurized. The graft is typically either sutured or adhered to the inside or outside of the stent depending on the device.

While a few devices rely entirely on passive fixation all devices incur at least some passive fixation between the SG and the arterial intimal surface even if they utilize active fixation techniques. This passive fixation is induced by sizing the SG slightly (typically 10-20%) larger than the nominal diameter of the artery (oversizing) prior to crimping, insertion and deployment. Oversizing (OS) is common practice and manufacturers typically have a range that is recommended with each device. Oversizing is perceived to benefit a graft in conforming to tortuous vasculature and reducing the occurrence of migration by increasing the attachment strength thus what is called the pullout force. Oversizing under 10% has been show to increase the occurrence of type I endoleaks [21]. Sternbergh [29] showed that oversizing above 30% adversely increased the

Proximal Barbs

Figure 3: Excluder with proximal infrarenal barbs.

Source: W.L. Gore (www.goremedical.com). Available from: (http://www.goremedical.com/newsletters/peripheral-vision/issue-2/news1.html)
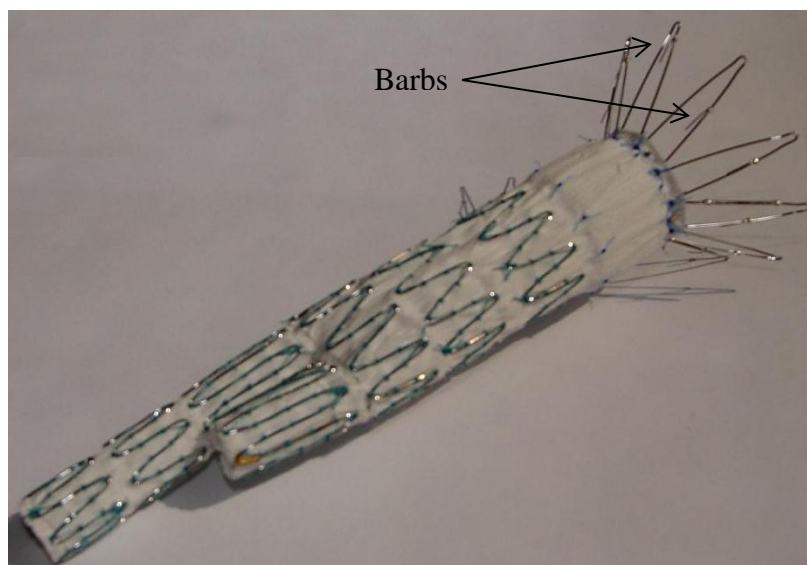
Barbs

Figure 4: Zenith EVG showing flared suprarenal stent with barbs.

occurrence of migration (> 5mm) by ~14 fold at 12 months using Zenith (Cook Medical, Bloomington, IN) grafts. A number of newer (early 2000s on) devices independently or in conjunction with passive fixation utilize active fixation designs which include angled barbs located on the proximal graft stent (Figure 3) or on flared proximal stent segments (Figure 4). The use of these barbs has been shown to positively influence stent graft performance with respect to increasing pull-out force[18,25]. Table 1 and Table 2 summarize the EVG devices and their FDA approval time, material selection, barb location, and fixation type.

Table 2: Relevant device design considerations.

Graft Name	Graft Material	Fixation Type	Proximal Fixation Loc.	Barb Location
Excluder	ePTFE	Passive/Active	Infrarenal	Infrarenal
Zenith Flex	Woven Poly.	Passive/Active	Suprarenal	Suprarenal
AneuRX	Woven Poly.	Passive	Infrarenal	None
Talent	Woven Poly.	Passive	Suprarenal	None
Endurant II	Woven Poly.	Passive/Active	Suprarenal	Suprarenal
Powerlink	ePTFE	Anatomical/Passive	Supra/Infrarenal	None
AFX	Multilayer ePTFE	Anatomical/Passive	Supra/Infrarenal	None
Ovation	PTFE	Passive/Active	Suprarenal	Suprarenal

The fixation of a stent graft is directly related to migration but not sealing which is influenced by the radial force in the proximal segment of the stent graft. Migration is

typically caused by fluid drag forces being larger than fixation forces but certainly device material failures could also allow migration. Some devices like the Excluder (W.L. Gore, Flagstaff, AZ) utilize a proximal sealant ring to create the radial force to inhibit type I endoleak. While this will induce some passive fixation as well the Excluder and a number of other devices carry most of their migration resistance by the employing of barbs. Though there is some overlap by the occurrence of oversizing, fixation is usually considered independent of sealing. They are related post deployment by the fact that if a SG migrates, it is likely to change the quality of the proximal seal and potentially increase the opportunity for a type I endoleak. Alternatively an endoleak could occur first and then influence the stent graft to distally migrate but Zarins et al. noted that post-procedure endoleaks were not significant predictors of migration [35].

<div align="center">Motivation for the Project</div>

Endovascular aneurysm repair techniques have given rise to a noninvasive treatment. This allows patients who lack the health for surgical repair a treatment option and those patients who meet a selection criteria a reduced chance of short term morbidity and mortality complications. Yet the very opportunity for this to exist as an alternative is built upon the ability of the stent graft to undergo extreme deformation when placed into a catheter and then radially expand to meet the arterial wall at the time of deployment. Once in contact the device must; maintain a good apposition with the artery in order to seal blood from the lumen of the aneurysm, resist migration and channel blood from the infrarenal aorta to the iliac arteries.

The mechanics at the point in time of deployment are quite complex as is the interplay between the artery and device is hinged upon the design of the stent, the graft, barbs and how they are all bonded together. Clearly there is an interface pressure that exists between the outside of the stent graft and the intimal layer of the artery. This is induced by the oversizing selection. When the graft is initially collapsed in the catheter it

has its maximal potential energy. Once it is deployed from the catheter and contacts the artery wall the graft will begin displace the elastic artery and at a given point come to equilibrium with the artery. At this point the graft is not fully expanded as it would be if in ex-vivo conditions due to the artery resisting its radial expansion. That is, the artery pushes back on the stent graft until equilibrium is achieved. This is the root of the existence of interface pressure which plays a role in both proximal sealing and migration resistance.

The long term fixation and sealing characteristics (durability) of even newer stent grafts, though unknown, is likely related to the nature of its apposition to the aortic wall. Currently there is little understanding of the mechanisms and factors involved in the how the device performs in conforming to the aortic vasculature and its nature in the fixation and sealing process during deployment. Such factors as neck angulation, calcifications, stent design and oversizing are all of particular relevance. It is likely that manufacturers may look at some of these considerations and have required values of radial, crimping forces and fatigue based performance criterion that must be met as design requirements and quality control, though this is not published public data. Additionally the testing methodologies may vary between manufacturers. As such, the experimental procedure may not account for the gestalt mechanics the graft undergoes when under full three dimensional compression. The development of an experimental methodology to capture this behavior and the construction of a finite element model, if established with rigor, can be advantageous in gaining insight into these mechanics and probing the interactions of these factors.

To construct a representative finite element (FE) model that reflects the true nature of the endovascular graft requires experimentally derived data on its radial compressive properties. This data is relevant and though it does not attain the actual interface pressure, it does capture the characteristics of the endovascular grafts apposition to the aortic wall. For instance, if the graft were to be radially stiffer due to a thicker

stent wire it would apply a higher force on the aortic wall thus a higher interface pressure as compared to a more compliant graft. This and other possible scenarios would certainly change its fixation and sealing characteristics. To our knowledge no one has published such data that captures the radially compressive properties of endovascular stent grafts induced by a three dimensionally based form of loading.

The overall objective of this work is to develop a finite element model of an endovascular stent graft. To accomplish this objective, the following specific aims were developed:

- To formulate an experimental methodology that captures the radial compressive behavior of an endovascular stent graft.
- To develop a fully parameterized finite element model of the stent structure that permits easy modifications to parameter based geometric characteristics such as diameter and height.
- To compare and reconcile the compressive behavior of the finite element model against measured experimental data.

CHAPTER 2: EXPERIMENTAL AND MODELING METHODOLOGY

Experimental Investigation

The goal in the experimental methodology is to capture the radial compressive properties. But there are multiple ways of studying these properties and they depend on the method chosen as well as the implementation of that method. As such one can surmise that there are theoretical tradeoffs for different pursuits. These are described in the following section.

Method 1: Liquid Based Compression

As seen in the side cross-section schematic in Figure 5 below the stent graft is encapsulates in a thin polymer membrane which is sealed inside an acrylic box that is filled with water. The water column pressure applies the external force on the graft
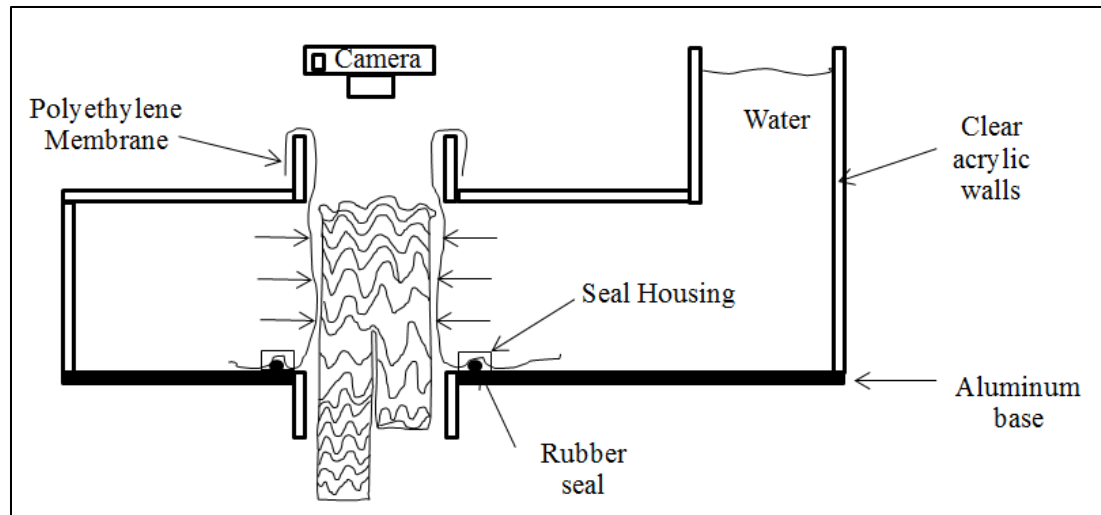
Figure 5: Experimental consideration for radial compression using water as the pressurizing fluid.

causing it to collapse. An image of the graft lumen would be collected at varying water

column heights in order to attain the pressure-driven deformation. The pressure could either be collected by calculation or by a pressure sensor. The challenges to this approach that were considered included the need to get good seals with the polymer sleeve. Achieving adequate images of the graft to approximate the diameter change under varying compression was also of concern. Additionally, the amount of exposure of the graft to the fluid pressure could be a limiting challenge if the graft had a tendency to slip from its intended position within the polymer membrane.

Method 2: Sequential Deployment in Compliant Tubes of Increasing Diameter

Figure 6 illustrates the idea of utilizing a polymer tube as the construct to find the estimated interface pressure. The progression of this method would be to first deploy the

Step 1: Deploy SG

Step 2: Measure diameter change

Step 3: Remove SG

Step 4: Apply internal pressure to

equal diameter change
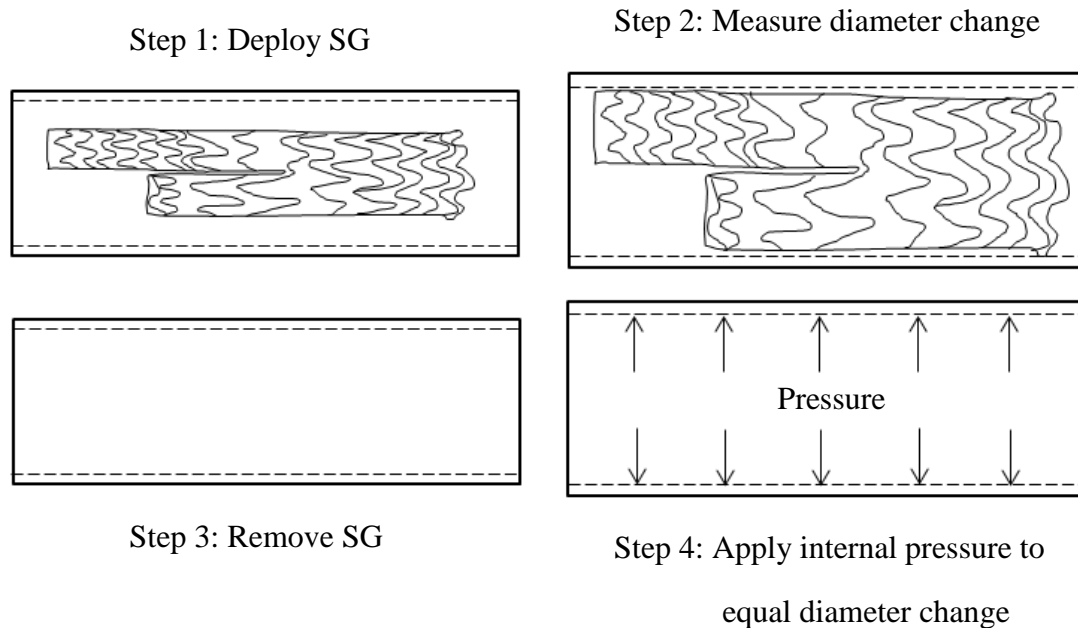
Pressure

Figure 6: Experimental consideration for radial compressive properties using multiple silicone tubes with varying inner diameters.

endovascular graft into the polymer tube and then measure the amount the tube was radially displaced by the expanded SG. The device would then be removed, one end of the tube would be sealed and the polymer tube itself would be pressurized through a sealed port on the other end. When the positive internal pressure displaced the polymer tubing to the same diameter the SG achieved, that would be the equivalent anticipated interface pressure. To get a plot of the pressure displacement response polymer tubes of varying internal diameters may be used to obtain the pressure-radial displacement data. This could have been achieved in several ways; by varying the polymer modulus with a constant wall thickness and inner diameter (ID), by changing the wall thickness with a constant modulus and ID or as suggested by varying the ID with constant modulus and wall thickness. For our proposed scenario a challenge was in estimating what the effect a small change in internal diameter would have on the displacement. This effect may be non-linear so a large count of polymer tubing constructs initially with small ID increment designations may have been required to get a reliable (low noise) pressure-diameter curve. The larger internal diameters on the other hand may have only required a few ID variations spread over a wider span in order to achieve an adequate density of data points. Visual confirmation of the device in the tube was deemed necessary to verify a proper deployment without effects such as folding. A clear and compliant silicone was considered adequate for visual inspections. The effect of wall thickness of the tubing on the deformation of the endovascular graft needs to be considered[32]. In fact it is likely the case where a thicker, though still compliant wall may be more inclined to attenuate any non-uniform behavior of the graft in compression. This also means that the estimated interface pressure may likely be less uniform as some local segments that want to freely deform have an increased radial resistance due to the tubing attenuation effect (or radial resistance to non-uniform radial deformation).

Method 3: Direct Interface Pressure Measurement

The use of pressure sensitive film or flexible pressure sensors currently available on the market was considered. They would be used to directly measure the contact or interface pressure between the stent graft and an elastic tube. The tubing would vary in internal diameter or wall thickness as was considered in previously in order to get a pressure diameter response interval. Similar challenges to those in the previous consideration apply here in non-uniform compressive response attenuation. A couple of other major challenges with this concept included sensor resolution, sensitivity response and cost. Finally, if this were pursued it would capture the actual interface pressure which certainly would not be uniform. While interesting and possibly beneficial in the study of endovascular devices it may have proven to be less advantageous in constructing and validating a computational model that mimics the compressive properties of the SG. A follow-up study could be performed with the validated model to see how well the model matches with this interface pressure map but this would be for a future work.

Method 4: External Sleeve Compression

The experimental method we selected to attain the pressure-diameter response of the stent graft is illustrated in Figure 7. The basic principle of the experiment is to cover the stent graft with an air-tight compliant sleeve and subject it to negative pressure while recording the reduction in its size. The sleeve relies on thin 2 mil polyethylene tubing (LDPE) as the construct to impute the vacuum pressure on the graft. The stent graft was inserted inside the polyethylene tubing which was approximately 3 times as long as the stent graft on either side. A rubber corks was used on one end of the sleeve while general and hemostatic valves were used on the other end in conjunction with polymer tubing to make the graft-sleeve complex airtight. A Millar Mikro-tip (Millar Instruments, Huston, TX) pressure catheter, connected to a computer with a LabVIEW (National Instruments, Austin, TX) data acquisition system, was inserted through the tube using the hemostatic

valve. The pressure transducer was validated against mechanical pressure gauges to verify its calibration (Figure 8). A simple Luer lock valve access was also used to
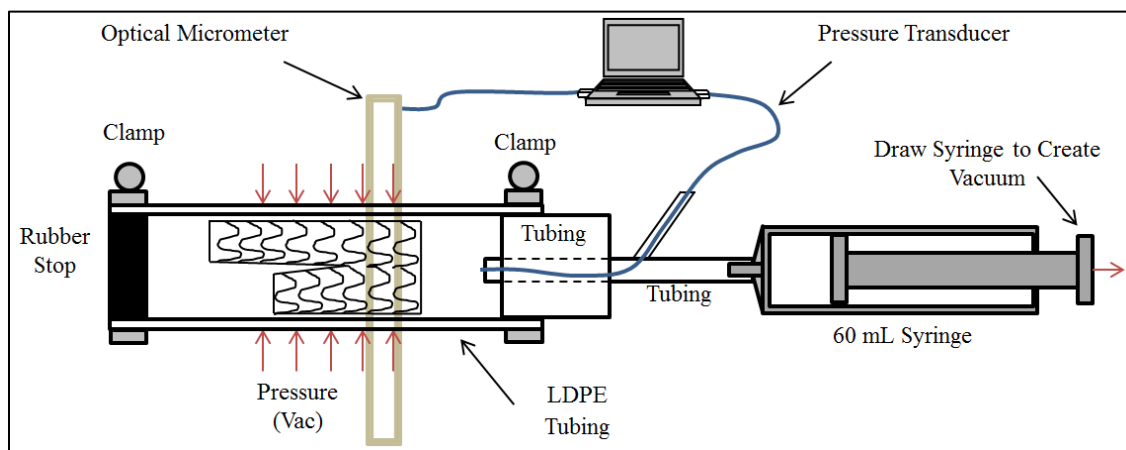
Figure 7: Schematic shows the experimental setup used to capture the compressive properties of the Excluder stent graft.

connect a syringe in order to manually apply the vacuum pressure. At the proximal end of the stent graft the supporting tubing extended into the sleeve in a tapered or staged manner as it approached the graft. This tubing was positioned to remain 1-2 cm away from the stent graft. This was selected as a means to reduce the edge effects of the sleeve rolling the edges of the stent graft down when undergoing compression. The proximal end of the LDPE tubing was fixed in place while the distal end was free to slide reducing any longitudinal tension in the tubing, thus minimizing any effect on non-uniform compression along the graft axis. A Keyence LS-7600 (Keyence Corporation, Osaka, Japan) optical micrometer was used to measure the sleeve diameter during compression. The temperature was controlled between 99-101 ^{o}F using a wafer style mechanical
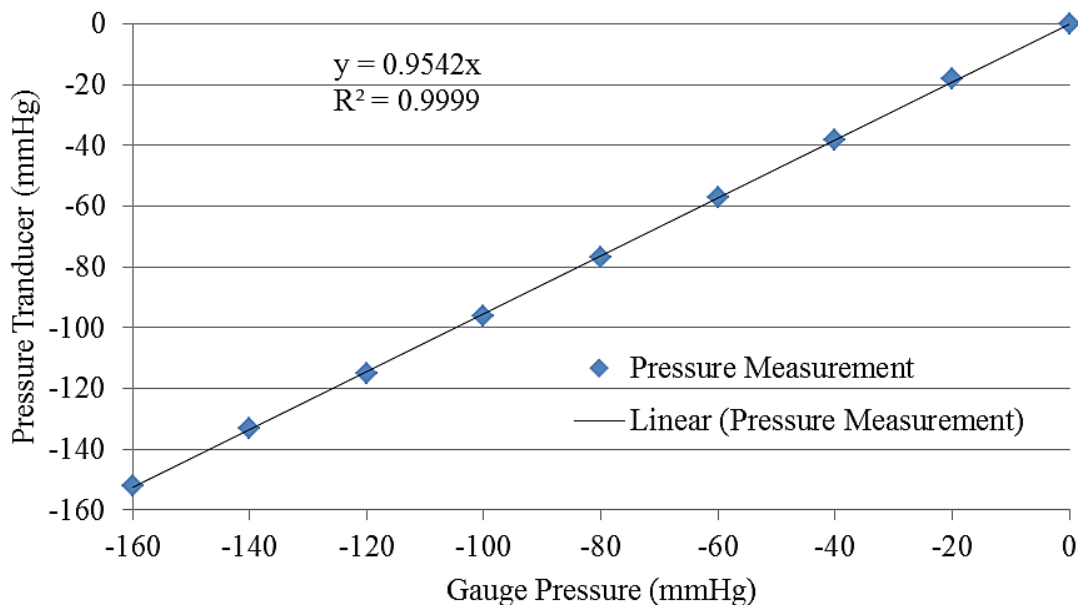
Figure 8: Plot showing Millar Micro-tip pressure catheter transducer validation against mechanical gauge.

thermostat wired in series with a 1500 watt convective heater. A plywood box with front acrylic slide out access and a translucent plastic top was used as housing for the experimental setup. This allowed easy access and enough light exposure to adequately see while still containing the generated heat. The electrical components for the DAQ hardware and laptop were located outside this housing and the heater was located inside it. Figure 9 provides a picture of the actual layout. Ten independent Excluder endovascular grafts were used for testing after the removal of proximal barbs. Initial zero pressure and diameter measurements were taken prior to the start of each compression. While recording the pressure and diameter changes, the syringe was manually drawn to create a range of negative pressures until the stent graft underwent complete compression. Pressures ranged from 0 to -55 mmHg over a period of approximately 2.5 minutes (loading). Subsequently, the syringe was compressed to re-pressurize the sleeve-
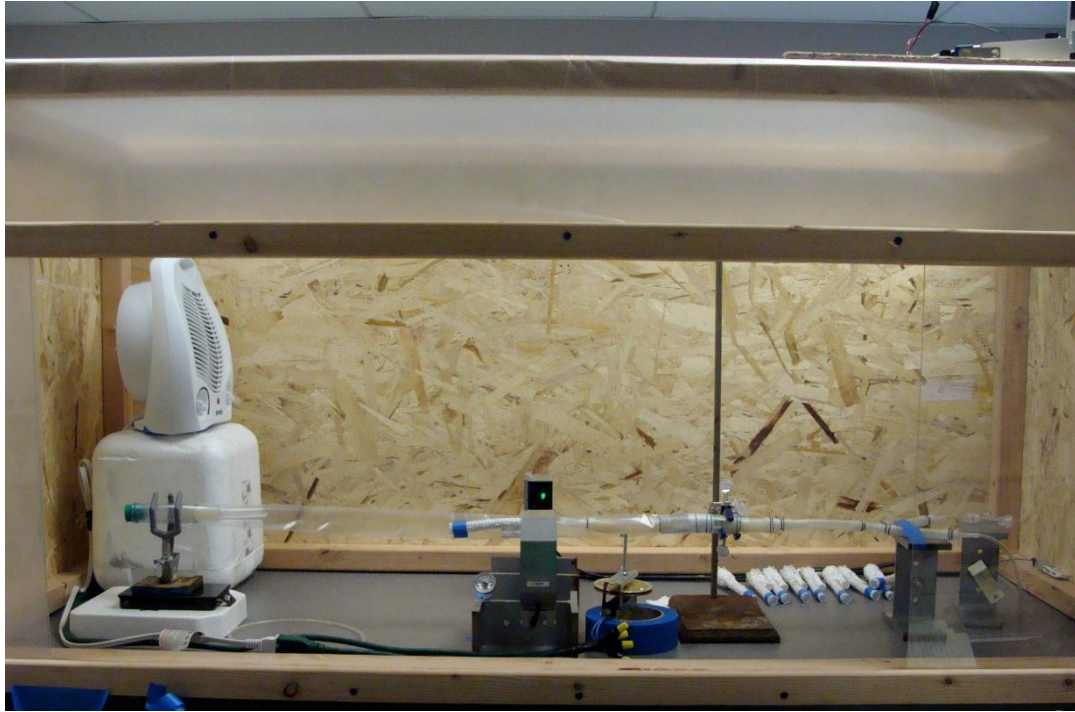
Figure 9: Lab experimental setup.

graft complex until zero pressure was reached over another approximately 2.5 minutes

(unloading). All the data was collected at the rate of one data point per second. The test

was repeated by rotating the SG 90 degrees such that the plane of bifurcation is parallel to

the plane of the optical measurement in one iteration and perpendicular to it in another.

This was done because the compression of the SG was not concentric but rather elliptical

in nature. The two orientations allowed us to measure the change in dimension along

both the medial-lateral and anterior-posterior directions.

Development of an FE Model of a Stent Graft

The FE model of a SG involves the geometry of the stent, the ascribing material

behavior and the boundary conditions. The geometry was formulated from an Excluder

device on hand while the material behavior and boundary conditions were derived from

the acquired experimental data and experimental setup respectively.

Formation of the Stent Geometry

The goal was to build a rudimentary stent only based FE model of the stent graft that reflects the experimentally measured negative pressure-diameter relationship for the commercial Excluder stent graft. The geometry was constructed in a bottom-up style approach in two separate models, a simplified model and a complex model. In this approach one typically starts with the most basic model based entities. For example a series of keypoints can be generated and a spline or line can be fit to these points in space. Following these steps the areas are generated from the lines and volumes are later created from these areas. A top-down approach would be to create the areas and volumes directly using built in functions within given software.

A very rudimentary model was initially constructed with eight equally spaced peaks and four continuous coils. This was done from an actual graft on hand and the amount of coil drop per revolution was measured between the top four stents and then
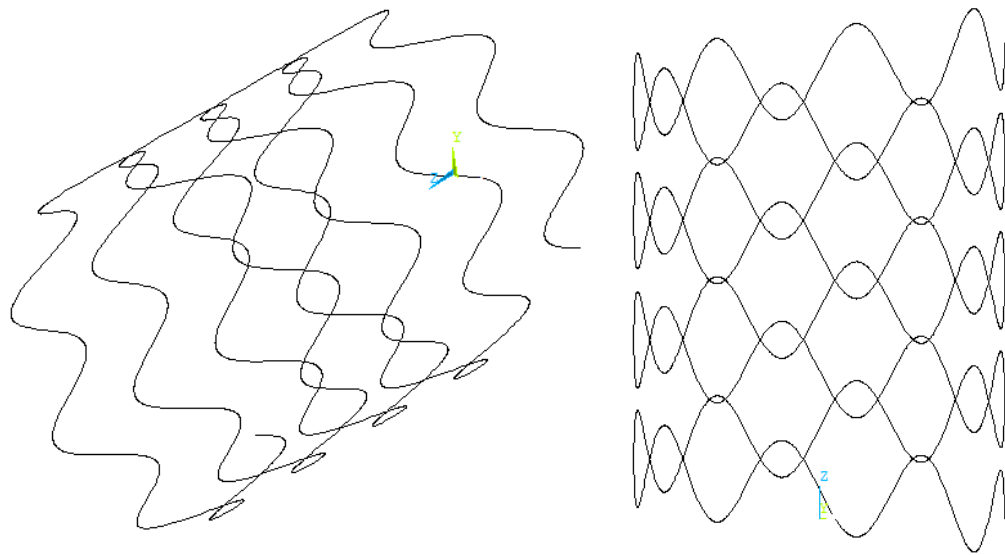
Figure 10: Simplified stent geometry imported into ANSYS.

averaged. The coil amplitude was also averaged and all measurements including the stent diameter were taken with an optical micrometer. Figure 10 shows the simplified geometry model of an Excluder stent that was created in ProEngineer using a 3D cartesian based curve definition. This spline curve was then imported into ANSYS (ANSYS Inc., Canonsburg, PA) as an IGES file.

A second and more rigorous model was then created using the APDL command set available in ANSYS. The stent geometry was created using a script file and builds upon parameterized input variables. Such inputs allow the user to easily adjust variables: wire diameter, number of peaks per coil, coil amplitude, wavelength, coil height drop per revolution, number of coils, and proximal body and leg diameters among others. This is advantageous in that it allows for quick stent 'architecture' design changes with fast turnarounds for FE model analysis. In doing so one can setup a conditioned scenario and then quickly and easily adjust the stent design to see how it will effect the performance of the stent in that given setting.

The initial process of creating a more thorough model of the Excluder SG was to first determine the stent path. The main body of the stent graft was selected to be aligned vertically with the z-axis where the stent path is then organized so that it revolves about the z-axis in a clockwise progression starting at the location of z =0. This was done using the space vector equations in a do loop iterated through 't' based increments for each coil. Appendix A shows a sample of the script that generates the first coil. Here 'HEIGHT' is the z-axis height drop at each increment (multiply by $2*\pi$ to get the total drop for a given coil revolution). The designation of 'AMP' is the amplitude of a single coil or the amplitude in a specific coil segment; varying amplitudes did occur within most coils. The 'PEAKS' defines the number of peaks per coil revolution and the "SPACING" sets the z-axis offset for the start of each coil. Also, 'dt' is defined as 2*PI/(POINTS) where "POINTS" is equal to PEAKS*16. Thus, for the Excluder SG there are 8 peaks and thus 128 keypoints designated to define the pathway for each coil. Yet, using these equations a

series of 'j' keypoints are actually created for each coil or rather one keypoint for each increment. The 'j' iterator is used as some coils segments do not have the full 128 keypoints due to path line changes. For example using the above parametric equations Figure 11 shows a screen image of the first set of keypoints created in the clockwise

Figure 11: The keypoints generated for the first coil
of the actual Excluder stent.

manner about the z-axis for the first coil. A total of 9 coils are generated in a helical manner and are initially created in a cylinder fashion with a constant radius. An additional two leg coils are also generated at the distal end of the SG. One of these is the conclusion of the ipsilateral leg. The other is an approximation of the contralateral leg which actually continues distally but the model geometry was simplified at this point. This simplification is believed to be acceptable as the area of interest is in the proximal region rather than the mid or distal segments of the SG. Once the keypoints are generated splines are then fit to each coil. Figure 12 illustrates the process of generating

a spline through the keypoints. When fitting a spline to keypoints, ANSYS has a maximum of 200 keypoints that are allowed to be selected. In the best work around to this and to make smooth transitions between amplitudes of one coil and the next, we
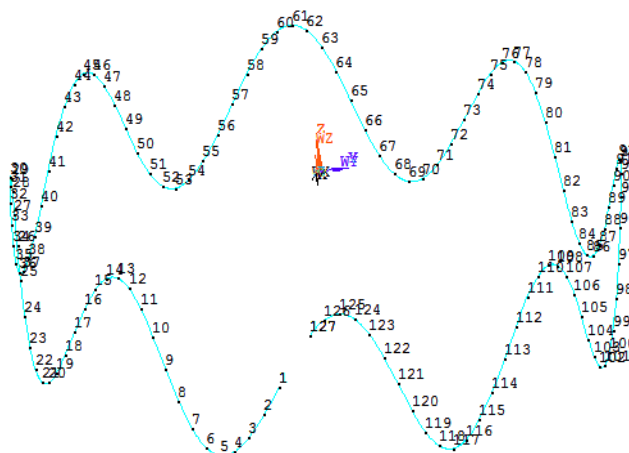
Figure 12: Spline created through keypoints.

selected each coil spline to start near a given coils first lower apex and finished near its last upmost apex (Figure 13). Then, seven keypoints are linearly filled between the ending of the prior coil and the start of the next. The splines were then selected to end on a given coils primary keypoints plus four keypoints while starting the next spline on the keypoints starting the next coil but four keypoints back. At this transition point the line ends and becomes discontinuous, so linearly filling with keyponts helps by smoothing any major C^1 discontinuities that would certainly occur in the transition from one coil to the next. Figures 14 and 15 illustrate the practice employed to ensure a 'best fit' C^1 continuity through the transitions. Though Figure 15 does not have the transition point in the same place as Figure 14 due to keypoint locations, it does portray how much

movement the pathline undergoes without the smoothing. For large amplitude

fluctuations between the end of one coil and the start of the next this effect becomes

magnified. Because each of the top few coils essentially has 127 keypoints one option
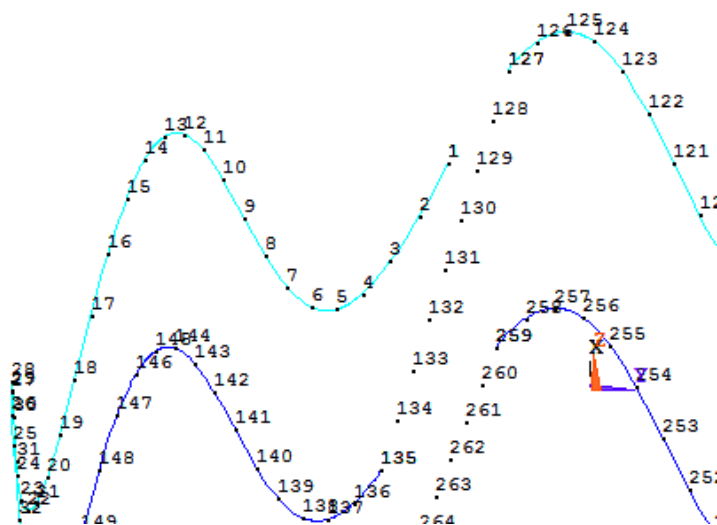
Figure 13: Splines showing starting and ending
locations.

could have been to select the transition at a later point. In this case a single spline would

contain all of a given coils keypoints plus part of the keypoints for the following coil. As

well, one could have selected an ending point less than all the keypoints in a coil as the

transition point. These options would have been troublesome as the amplitudes of

different wavelength segments varied not only between individual stent coils but even

within a single coil. Figure 16a and 16c show the smoothing procedure described for the

transitions in all the splines for all nine coils plus the two end leg coils. As well, it

illustrates the geometry of the stent up to this point.
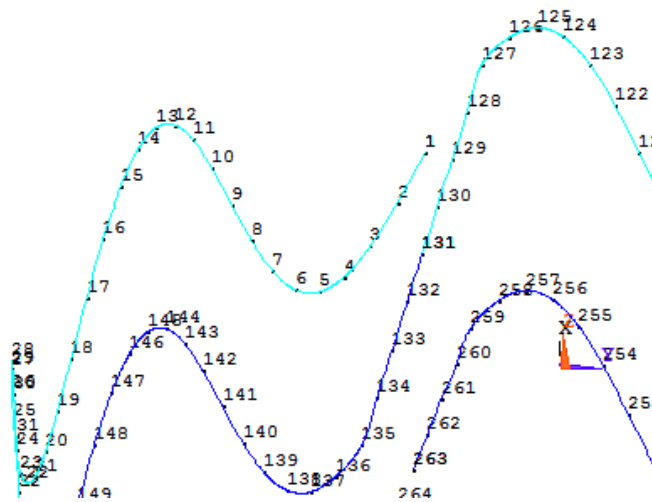
Figure 14: Final spline generation junction
between coils one and two.
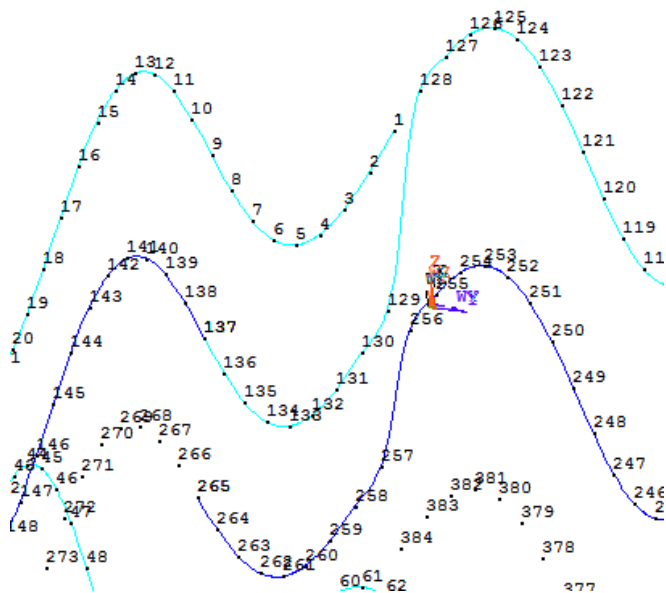
Figure 15: Illustration of the poor transitions
between coils without linear
smoothing.

a   b

c
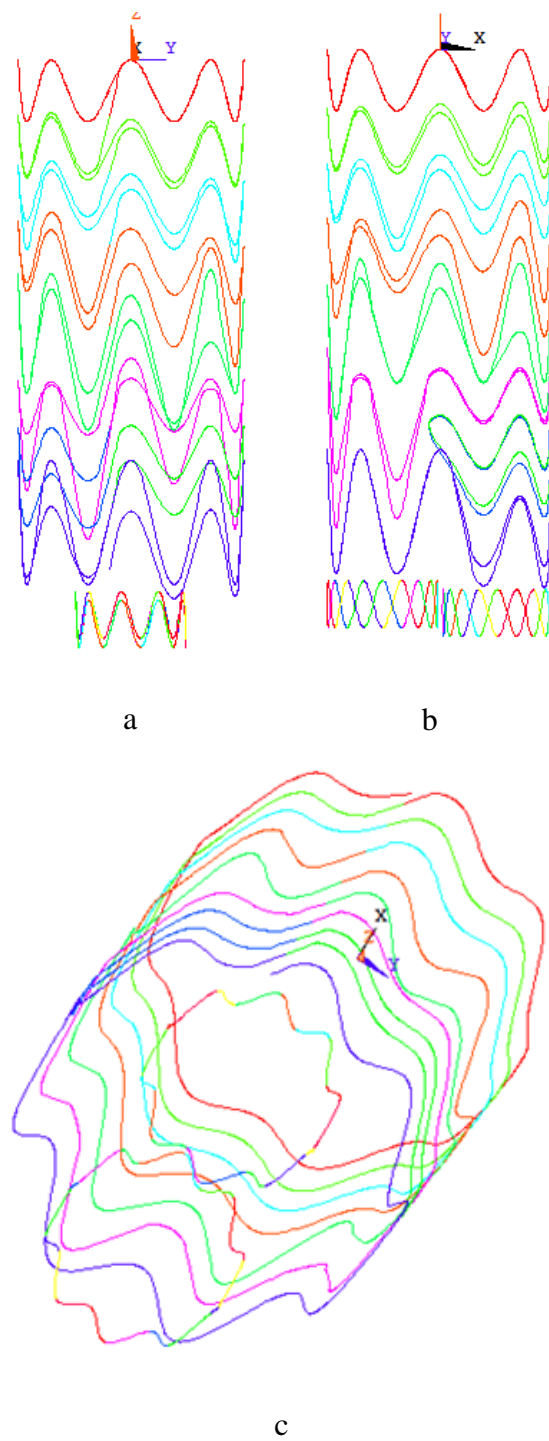
Figure 16: Stent pathline for nine coils.
      (a) Right sideview
      (b) Front view
      (c) Isometric-view

Once the splines were created they were shaped to the geometric form of the Excluder graft. Figure 16a depicts the right side view of the generated stent pathline with just the splines. Figure 17 shows what the right side view of the Excluder looks like. In
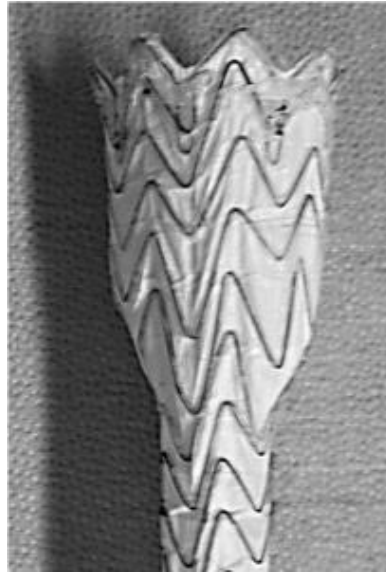
Figure 17: Right view of
Excluder SG.

order to get the front and back profiles to transition and taper as shown an upper most keypoint from the bottom troughs of coil four was selected and the radial location of the bottom of coil five was measured (which was set at the radius of the descending legs) from the device on hand. Using those as a reference the intermediate keypoint x, y and z locations were recalled and modified to linearly fill between the previously selected upper and lower keypoint locations using linear equations. One segment of coil four also included a similar set of steps but with different references. Figure 18a illustrates what the spline path now looks like after completing the tapering.
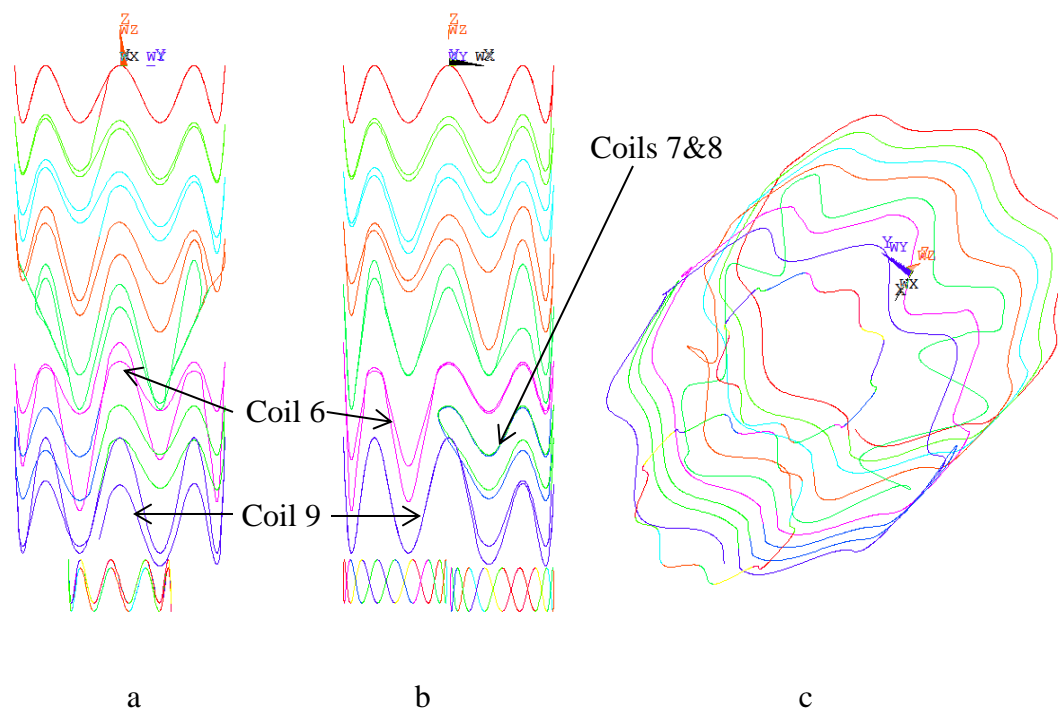
Figure 18: Spline tapering of coils 4and 5.
     (a) Right view
     (b) Front view
     (c) Isometric view

As seen in Figure 18a and 18c coils 6, 7, 8 and 9 all need to be configured to the diameter of the graft legs rather than their current which is the diameter of the proximal body. The ability to recall and modify keypoint x, y and z locations was again employed in order to achieve this. First the center of each leg was defined as 'offset' where offset = gap/2 + legradius (Figure 19). Then each equation for each quadrant of the smaller leg circles was defined. Solving for the y-location, the x-coordinate of the large circle was plugged in, and a new y-coordinate for the large circle was found at the given leg radius. In this step the original x and z keypoint locations all remained where they were originally located. This process actually takes the keypoints for the larger diameter and keeps the x-coordinate while modifying the y-coordinate to overlay the keypoint onto the
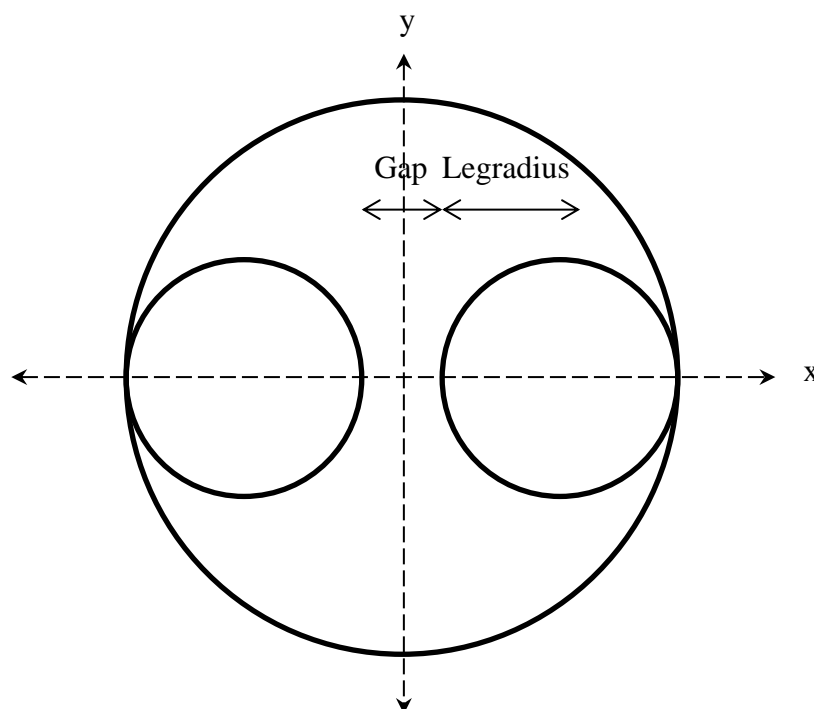
Figure 19: Top cross-section view of parameters used to create the stent legs.

graft leg. It would be analogous to mapping the spline by projection from a diameter of the proximal body onto the distal leg bodies. By doing so it retains an approximated stent wavelength as if someone had compressed the stent to fit against the graft leg during manufacturing. Had this process not been done this way and rather the stent pathline was generated initially along the leg diameter (keeping the number of stent keypoints and amplitude the same) the wavelength would have been incorrect. This outcome is illustrated in Figure 20 where you see the initial larger diameter coil wavelength and a second generated stent along the leg overlaid to compare the wavelengths. Another option would have been to rewrite the equations to match the appropriate new wavelength at the size of the leg radius but that would be more of a 'guess and check' approach in making sure the equations would be correct. It also would have been more
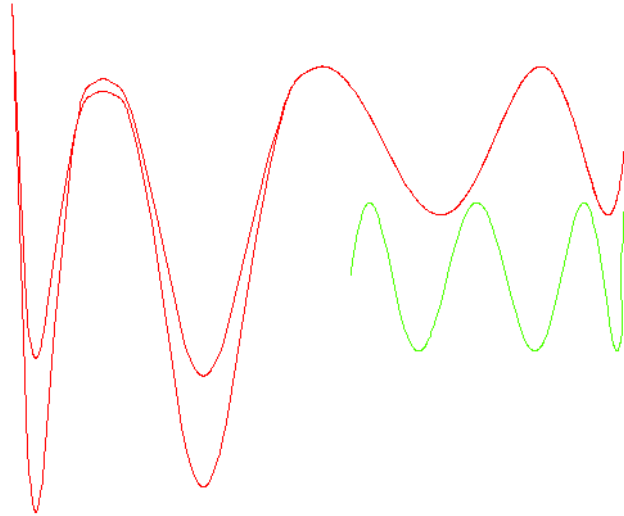
Figure 20: Difference between projecting initial
keypoints location (large stent) and
creating one with the same equations.

difficult to automate for stent architecture adjustments as each coil would need an

independent set of equations. All of these equations would then need separate parameters

for automation.

Once this was completed a digital caliper was used to measure the location of

each crest and trough for each coil. The script input parameters (amp, height and

spacing) were then adjusted so that each crest and trough was located within 1 mm of the

measured value. This 1 mm value was selected by general consideration and reasonable

estimation of the manufacturing variability. Figure 21 shows the finalized stent model

with the stent spline path shaping and parameter adjustments completed.

The aim was to construct a stent only model that mimics the dynamics of the stent

graft. An additional stent graft model was constructed as well for future use. In doing so

the spline path previously created was used to also generate the Excluder graft material.

In order to achieve smooth transitions through the curves and tapers three or four sided

areas were created. ANSYS then fit non-planar areas to these sides. To generate these
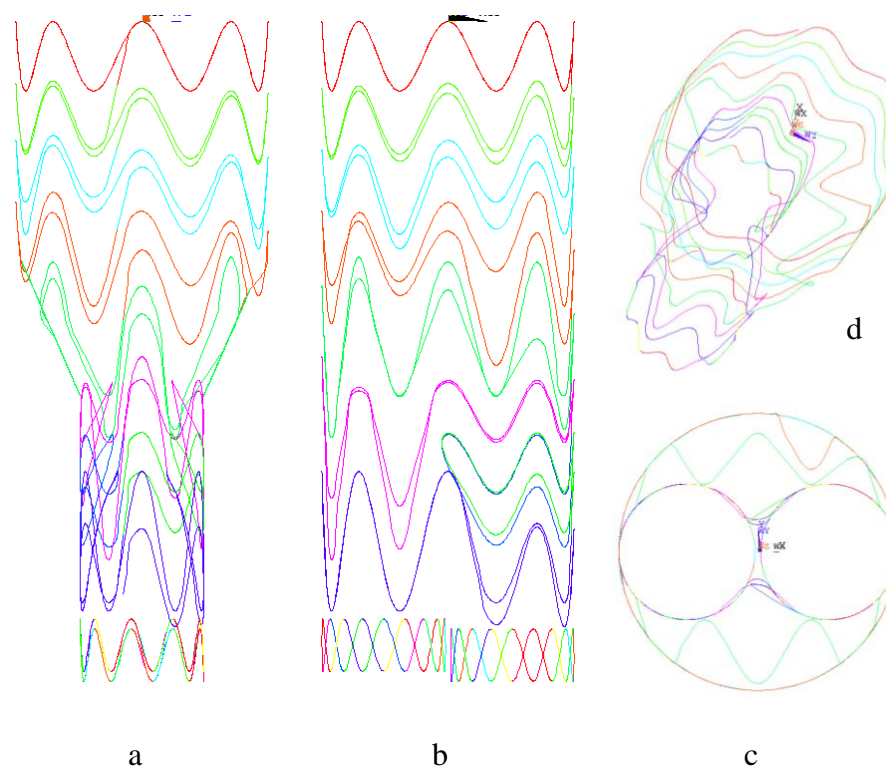
Figure 21: Final pathline for stent geometry.
(a) Right view
(b) Front view
(c) Top view
(d) Isometric view

areas the coils were segmented where every peak of the upper coil was vertically

connected to a peak of the ensuing coil located at similar x-y coordinates. The same

approach was done for each of the valleys. Then, one vertical line was additionally

created between each peak and valley of a coil and connected to the next coil at the

similar peak and valley x-y location. One could have created many more vertical lines

thus more area segments but again this approach seemed to create a reasonable amount of

area segments for meshing. Figure 22a details what has been described with more clarity
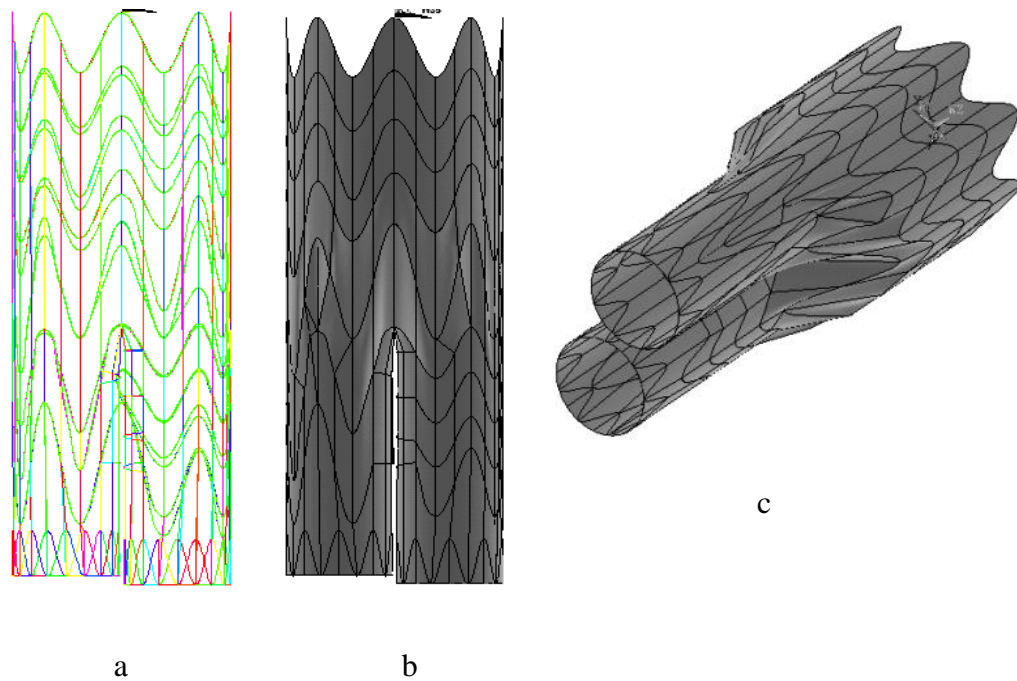
Figure 22: Area generation for graft material.
      (a) Vertical line segments
      (b) Front view of pathlines and areas
      (c) Isometric view of pathlines and areas

and Figures 22b and 22c show what this looks like when the areas have been patched in

place.

Sleeve Model Geometry Formation

The geometry for the sleeve was generated from two circles; one at the proximal

end and one at the distal end of the stent body. The diameters were the same and set just

outside the diameter of the stent graft. Initially the circles were subdivided into 16 arcs.

They were then combined so that the front and back each contained 6 arcs and the sides

each contained 2 arcs each. This left two sides that allowed for more refined meshes later

while the front and back could be coarsely meshed. The reason for the refined mesh was

based on expectations of the graft-sleeve complex to compress similar to the experiments which was not concentric. Finally, straight vertical lines were created between the beginning and end of corresponding arc. ANSYS was again used to create non-planar
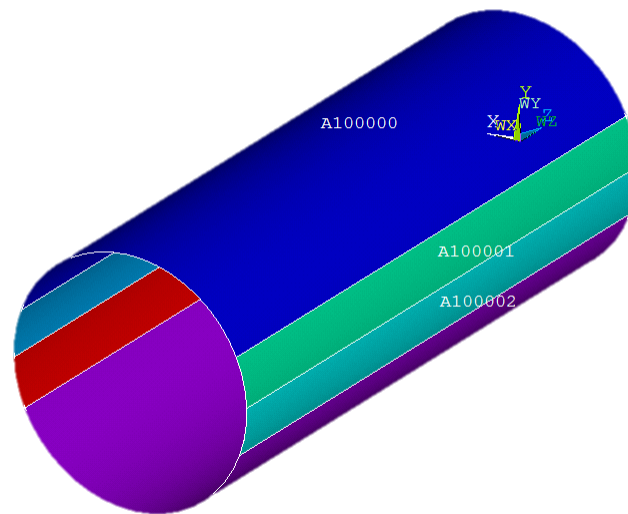
Figure 23: Modeled sleeve areas.

areas between these four sided lines in order to generate the sleeve material (Figure 23). In this case the sleeve front and side areas were not further segmented into smaller area sections as the cylinder for the sleeve was a smooth cylindrical surface and untapered, unlike the graft.

Finite Element Model Analysis

The initial simple four coil model was meshed in ANSYS with beam elements. The stent material was modeled as Nitinol in the fully transformed austenite phase with a linear elastic modulus of 40 GPa and poisson's ratio of 0.46 [31]. The pressure on the stent beam was calculated such that the total radial force on the stent is equivalent to that experienced by the graft surface (i.e. the measured negative pressure

times the contact surface area of the graft). Beam elements are loaded as force per length and so the total force on the stent was divided by the length of the stent prior to loading the stent elements. For boundary conditions, the keypoint on the right side of each coil where the keypoint x-coordinate value equaled zero was constrained in all degrees of

a   b
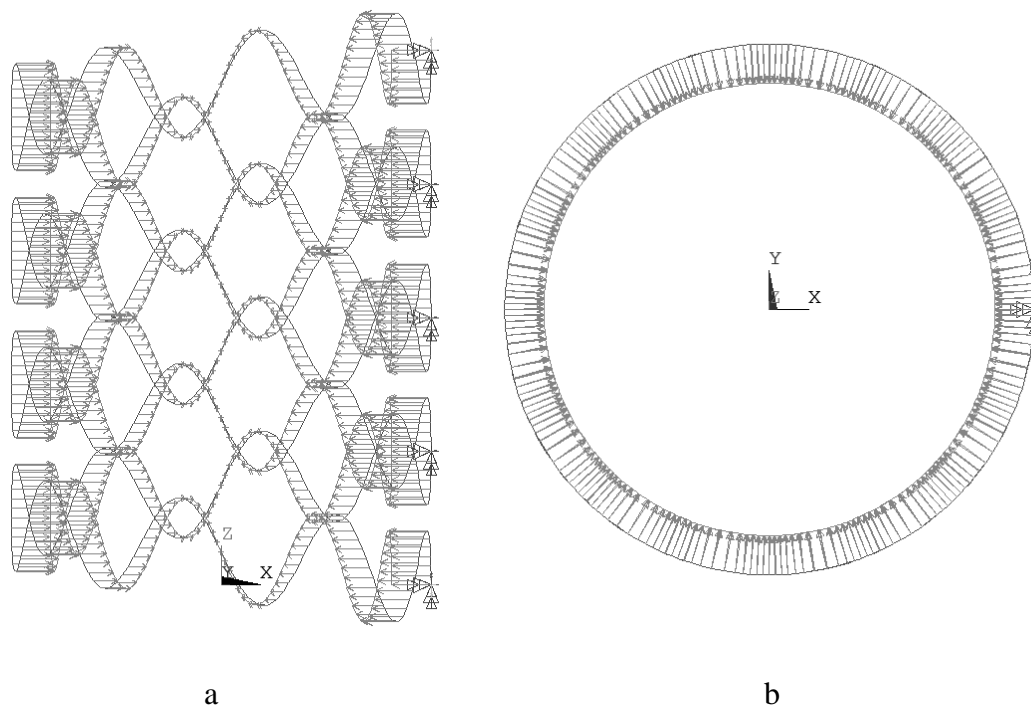
Figure 24: Loading conditions for the four coil stent.
      (a) Front view
      (b) Top view

freedom (Figure 24). A small displacement static analysis was completed on this stent model.

Meshing the more complex stent graft consisted of seeding the lines with varying element lengths depending on location and line length. Line verticals were set to an initial length of 0.18 cm and spline (wire) segments set to an initial length 0.08 cm.

These values were set while allowing the ANSYS mesher the ability to automatically adjust, if necessary, during meshing in order to optimize the mesh quality. Though a quadrilateral mesh is an option the mesh selected was a triangular free mesh due to the curvature and tapered nature of the graft. This resulted in a more uniform mesh from area to area. It also reduced the occurrence of localized spots where the mesh could result in very small densities during automatic mesh refinement. The final meshed stent
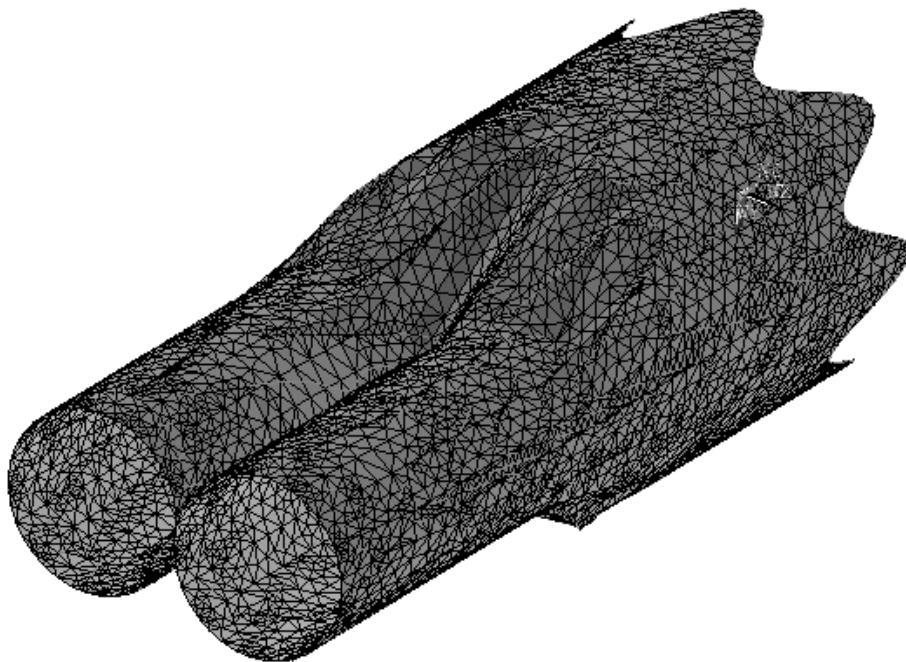
Figure 25: Fully meshed Excluder stent graft.

graft model is shown in Figure 25. Though elements were chosen in order to mesh the SG in ANSYS the node locations and element connectivity was exported and used as input data for Abaqus v.6.11 (Dassault Systemes, Velizy-Villacoublay, France).

The stent only model was derived from the stent graft model where only the nodes and element connectivity for the stent was exported to Abaqus. In Abaqus, B31 elements

were selected for the wire in both the stent only and stent graft models. The stent only model used shell S4 elements for the sleeve and the stent graft model used S4R elements for the sleeve and membrane M3D3 elements for the graft.

Two separate solution schemes were initially pursued with the representative stent
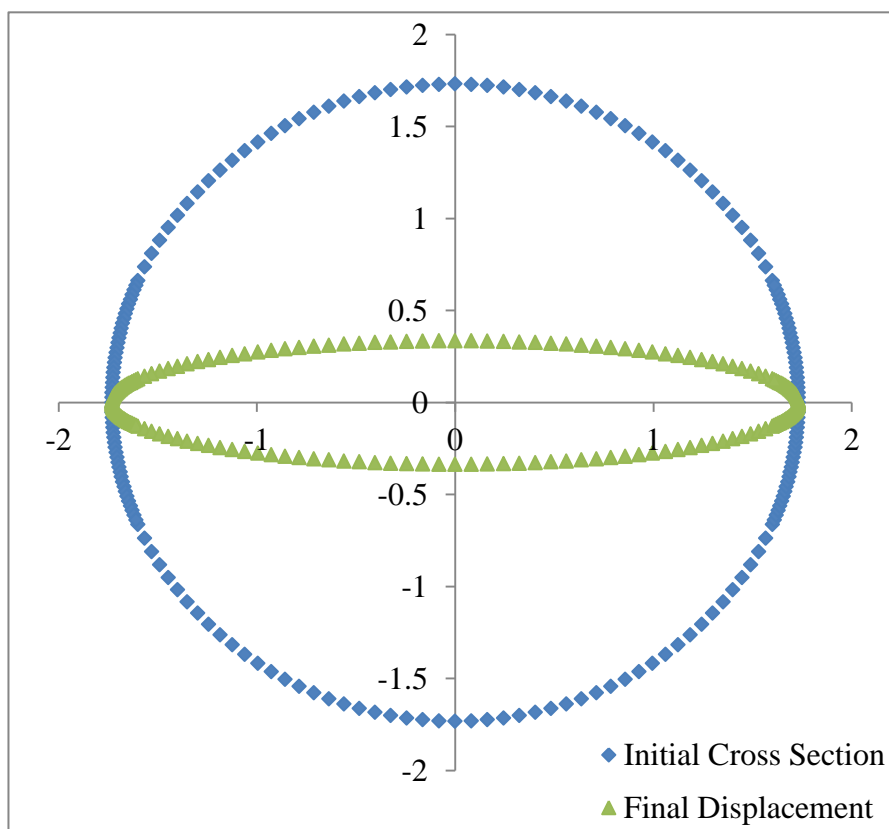
Figure 26: Displacement steps of the sleeve for the displacement driven solution.

only and the complete stent graft models; displacement based and force equilibrium contact analysis. The first scheme was a displacement driven response where the sleeve geometry started as a tube and the sleeve nodes were driven to deform as the experiments did through contact with the stent or stent-graft. Because displacement based problems

converge easier than force equilibrium contact models, this idea was laid out as the precursor to a force driven model. If convergence was attainable at this point then we would progress to the next (force based equilibrium) solution scheme. An excel plot shows how the sleeve is characterized by an ellipse based compression (Figure 26). This is done by mathematically driving each node in each x-y quadrant toward an elliptical form where the major and minor axis parameters were taken from the experiments. This first displacement based approach was utilized for large displacement static and also large displacement dynamic solutions. The former static based analysis was again a simplification in the process in order to achieve downstream convergence, mainly quasi-static dynamic based convergence. This is because a large displacement quasi-static dynamic solution scheme was used in the final force driven response. Thus, once convergence was achieved with displacement driven contact for the large displacement static condition we progressed to the same displacement driven contact for the large displacement quasi-static dynamic condition. When that was achieved the prior lessons learned in both the static and dynamic displacement solutions was utilized for force equilibrium contact in order to get the compressive pressure-diameter relationship. As mentioned, this final method was completed as a quasi-static dynamic force based contact problem using Abaqus standard.

In all scenarios Abaqus was allowed to choose the step size but suggested, time period of the step, minimum and maximum time increments were 0.001, 1,0.00005,1 respectively and the loading was completed as ramped rather than stepped. The initial wire diameter was set to 0.03 cm. The displacement driven problem used shell elements for the sleeve at a thickness of 0.00508 cm or 2 mil. The stent graft model used the same but also has membrane elements at the same 2 mil thickness for the graft material. All models with the complex geometry utilized node to surface based contact with no friction and a linear penalty for resolving contact overclosures. Table 3 summarizes the model scenarios pursued.

Table 3: List of solution methodologies that were pursued. The final and reported comparison to the experimental data is model four.

Model	Boundary Conditions	Solution Scheme	Model Components Included	Contact	Graft
1	Direct force on stent	Small displacement, linear elastic, static	Simplified stent only	No	No
2	Sleeve displacement	Large disp., linear elastic, static	Complex stent, sleeve	Node to surface	No
3	Sleeve displacement	Large disp., linear elastic, dynamic quasi-static	Complex stent-graft, sleeve	Node to surface	M3D3
4	Internal negative pressure on sleeve	Large disp., linear elastic, dynamic quasi-static	Complex stent, sleeve (S4 elements)	Node to surface, surface to surface	No

In the two intermediate models (2 and 3 in Table 3) the thickness of the graft and sleeve materials was measured with an optical micrometer, the density of the samples was found using a sample and a scale for the dynamic simulation (model 3) and material properties for the graft came from literature [31] and for the sleeve from MatWeb (matweb.com). Initially using the displacement driven solutions we anticipated varying the stent modulus in order to get the contact driven pressure diameter relationship to resemble the experiments. Yet when iterating through the increments that were recorded for each solution you see high localized contact stresses (Figure 27). The interpretation of these localized contact stresses could be quantified on a nodal basis and essentially
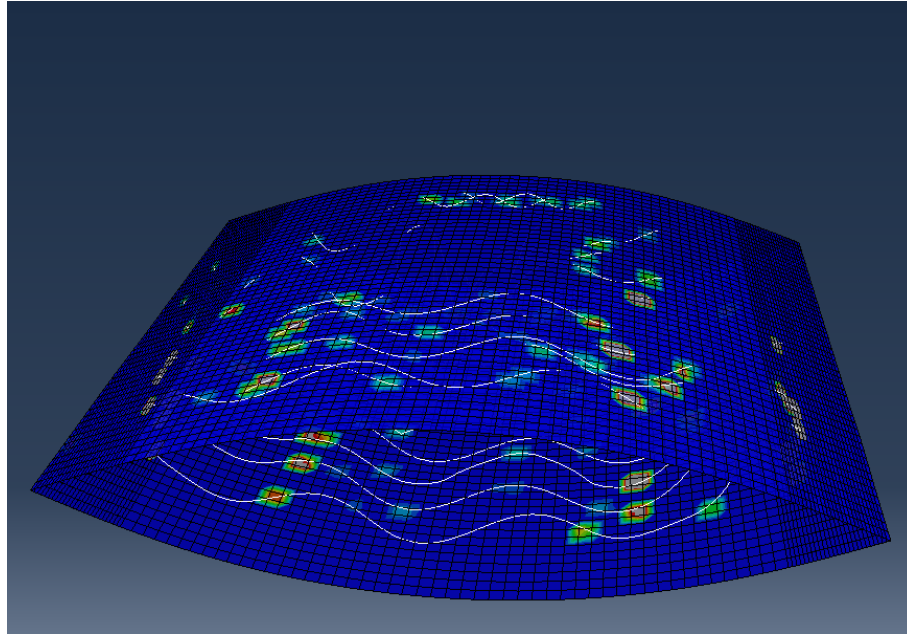
Figure 27: Nonlinear dynamic displacement driven solution scheme
for the sleeve and stent only. Plotted on the sleeve is the
nodal contact stress.

'averaged' in some manner across the graft contact area to give an estimated general

negative pressure. This would be an estimate at best. Yet it is difficult to interpret these

localized contact stresses in a manner that formulated the vacuum pressure as a whole

acting on the sleeve-graft complex at a given diameter. Given these challenges the actual

force driven contact was the route selected as it loaded the complex like our experiments.

In order to utilize a force equilibrium solution scheme we had to consider the

nature of loading the sleeve was undergoing. Primarily, we had to attain the response of

the sleeve itself to that of the experiments. To assume the sleeve to be responding to a

tensile stress based radial compression with linear elastic shell elements lead to a finite

element solution that required one to highly inflate the vacuum pressure in order to get

the sleeve to compress itself, let alone contact and compress the stent. The thin polymer

sleeve actually acts similar to a fabric but with more inertial resistance to bending.

Abaqus has a routine that allows one to define fabric like materials in Abaqus explicit but an explicit solution was outside the scope of pursuit for this project. As such one has to consider the effects of the compressive properties of the material in either a linear elastic or hyperelastic state, though they are by definition characterized by tensile properties. Reconsidering the sleeve from the experiment, it was used merely as a compliant air-tight material to create a chamber solely to transfer the vacuum pressure onto the stent graft. Having chosen an experimentally thin membrane thickness to begin with (2 mil) we were looking to see the response of the SG to negative pressure independent of the dynamic effects the sleeve may induced on the device or data. With this in mind we worked to attain the tensile properties of the sleeve but more importantly the bending properties of the sleeve. As mentioned in the experimental setup, one end of the tubing was fixed in place while the other was free to slide in order to reduce the axial tension in the sleeve while undergoing compression. While undergoing compression in each of the experiments, the free end actually slid approximately 1 cm. That is, some tension was incurred in the sleeve due to friction between the unfixed clamp base holding one end of the tube and the supporting surface. To find this tensile force an OHAUS spring scale was connected to the clamp body while dragging this same clamp along the same surface used during the experiment. The force was about 0.75 N and while the force just prior to slipping should theoretically be higher than the force during motion the resolution of this scale was not refined enough to resolve the difference. Worth noting is the fact that this motion occurred toward the middle to end of the loading (compression) cycle so the sleeve did not incur this total axial tension early in the compression but it did likely see some fraction of this force that would have varied with increasing vacuum pressure. With this information, ten rectangular samples (26.9mm x 60 mm) were cut from the polyethylene tubing. Each underwent a uniaxial force displacement test using Lloyd LF Plus (Lloyd Instruments Ltd., Bognor Regis, West Sussex, UK) uniaxial testing machine. The lower and upper clamps were vertically aligned and the extension test was set to pull

at a rate of 60 mm/min until the sample broke. A model of these polymer samples was generated in ANSYS with equal dimensions and a linear elastic small displacement solution was used to set the tensile elastic modulus. This was done by applying a force of 0.75 N to one end while constraining the opposing end and varying the modulus until the displacement matched the experimental average of the 10 samples. The corresponding modulus was 0.198 GPa. Comparing this to the tabulated data from MatWeb for extrusion grade LDPE shows it to be with the range of the modulus of elasticity for this material (0.152-0.290 GPa). Next the bending properties were evaluated. Three
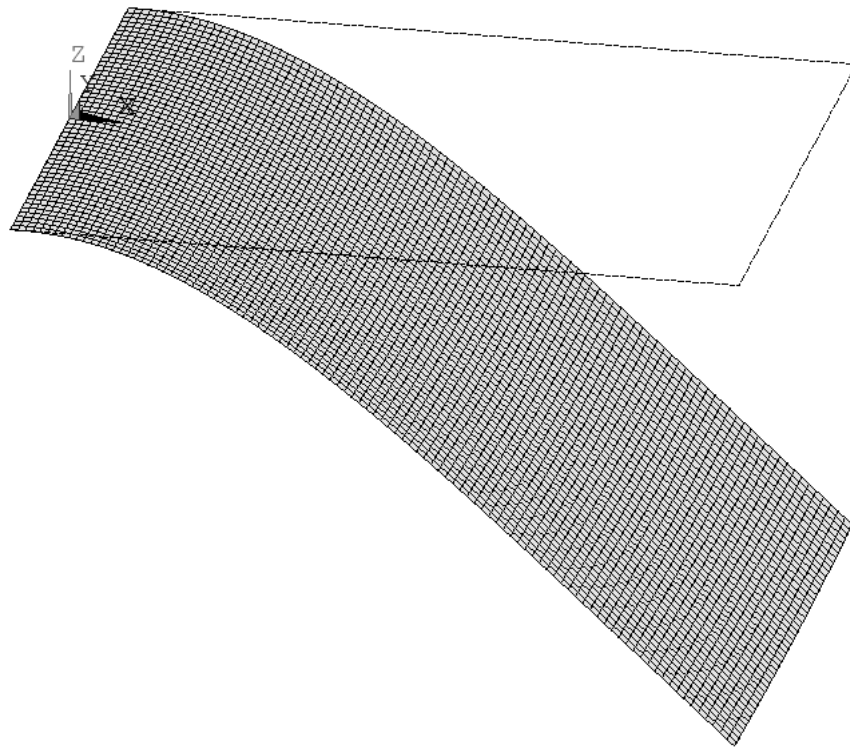
Figure 28: ANSYS plot where the bending properties of the sleeve are matched to experimental values using gravity as the external load.

rectangular samples (30 mm x 25.53 mm) were taken from the polymer tubing and placed in a horizontal clamp. The samples were allowed to deform under their own weight. As such smaller samples were needed compared to the tensile samples. This was because longer samples caused the weight to pull the sample nearly vertical each time which didn't allow one to measure the bending resistance. The vertical deformation was measured using an optical micrometer. Of the three samples the vertical distances they deformed were 24.3 mm, 24.4 mm and 24.2 mm. Again ANSYS was used to model the average bending of the polymer samples. The polymer model with the material properties previous set to match the uniaxial extension experiments was used. The dimensions were adjusted to match the polymer samples used in the bending experiment. Gravity was then induced as an external body load and a static linear elastic large displacement solution was initiated. Rather than adjusting the elastic modulus the material thickness was decreased until the deformation matched that of the experiments (Figure 28). After completing these experiments the material properties were E= 0.198 GPa, ν = 0.3 [33] and the sleeve thickness was 0.034 mm.

The boundary conditions for the force based simulation included constraining the right and left side nodes in plane with the bifurcation of the stent where the nodal x-value was 0 in the UY direction. This was selected because friction was not included to restrain the stents to not independently rotate thus it had an effect similar to the constraint as that of the graft material cohesively holding the stent to perform as a single device. All nodes of the stent were constrained in the UZ direction as the graft material also induces this constraint for all general considerations. The innermost location on the final leg coils were constrained in the UX and UY directions. In the experiments these inner legs contacted each other but self-contact with the stent was not included in the model. This condition simulated an effect of self-contact since the legs are nearly touching to start with. The nodes on the sleeve ends were constrained in the UZ direction. Finally the nodes on the sleeve ends where x=0 were constrained in the UY direction and the

nodes where y=0 were constrained in the UX direction. This was to help keep the sleeve from twisting during the solution and mimicked the experimental setup where though the sleeve was several times longer than the stent, the ends of the sleeve were bound to the tubing supports which didn't allow rotation. Surface-to-surface self-contact was initiated with the sleeve inner surface due to its large deformation. A pressure of a 35 mmHg vacuum was applied on the inner surface of the sleeve.

CHAPTER 3: RESULTS

Experimental Results

In each experiment, the zero pressure and corresponding diameter for a baseline measurement was captured. While none of the grafts were exactly the same size, in general they varied from minimum of 2.33 cm to a maximum of 2.77 cm in plane with the bifurcation and from 2.2 cm to 2.68 cm respectively in the orthogonal orientation. The ten stent grafts averaged a diameter of 2.57 cm in plane with the bifurcation and 2.44 cm orthogonal to this at zero pressure and measured with an optical micrometer. The
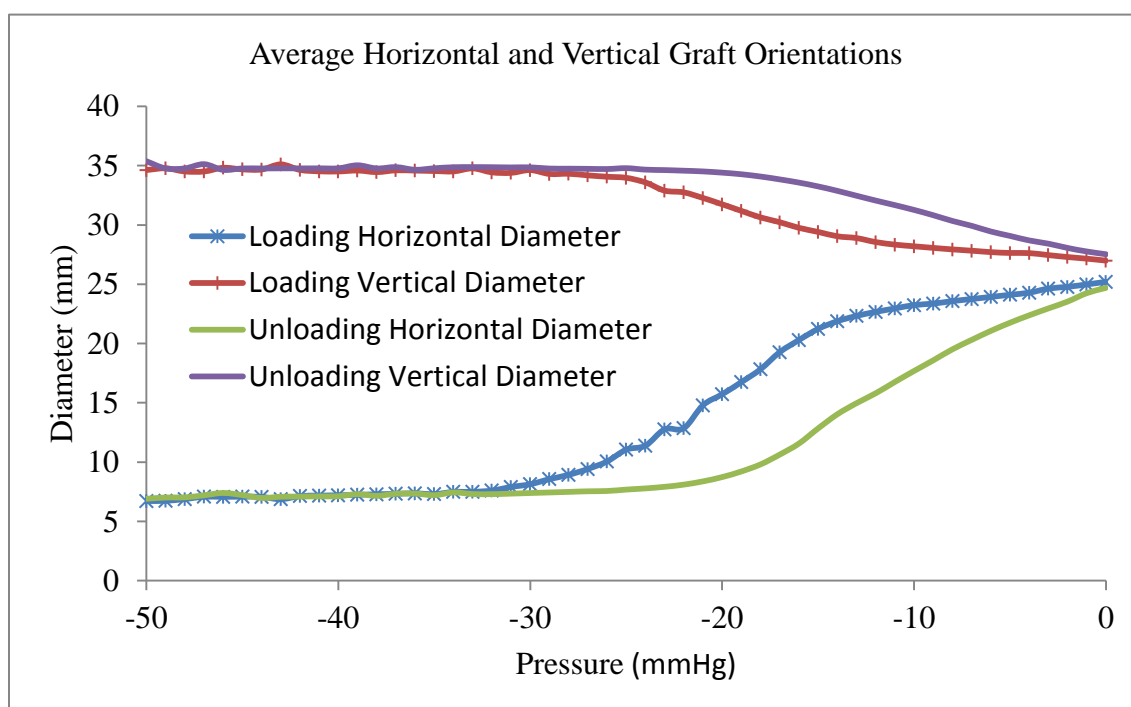
Figure 29: Average pressure diameter curves for experimental loading and unloading of the Excluder EVG.

radial compression of all ten stent graft devices was not concentric but rather elliptical with a minor axis (collapsing direction) consistently oriented along the anterior-posterior

direction. The raw data from all ten experiments shows where the increasing negative
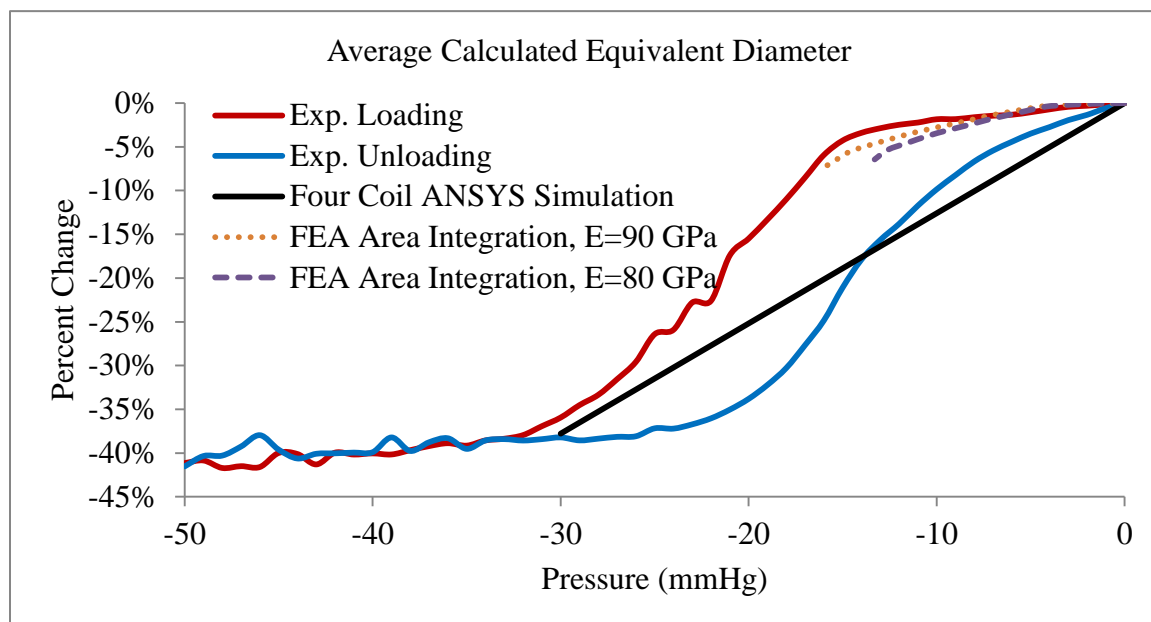
Figure 30: Equivalent diameter comparison between simplified and the complex model and the experimental values.

pressure caused a flattening of the stent graft with the minor axis asymptoting to near 7 mm. The major axis on the other hand increased in diameter during the compression. Figure 29 shows the average pressure diameter relationship of the raw data for the loading and unloading cycle to better display this occurrence rather than the raw data. The sleeve in Figure 27 shows the uniform quadrilateral mesh that was used. We selected to use this as the tracer for the cross-sectional area of the stent which our optical micrometers captured. As such, we calculated the area by integration of nodal x-y locations at a selected z-height, similar to where we measured in the lab, at a given pressure. We then equated this area to the area of a circle and calculated the diameter change for an equivalent circle. Having completed this, the data was normalized to

remove the variability of different graft sizes. Plot 29 shows this data averaged and normalized where the loading cycle asymptotes to a 40% reduction in equivalent diameter.   Also shown in the previous two plots is the hysteresis that the graft undergoes during the loading and unloading cycle.

<div align="center">Computational Results</div>

The simplified four coil stent had a starting diameter of 2.66 cm at zero pressure. The result for simplified four coil stent model with the small displacement static solution scheme is overlaid on the experimental results in Figure 30. This plot shows the average equivalent diameter of the experimental stent graft had is compressed concentrically. The model shows a linear response during the loading cycle and represents true symmetric
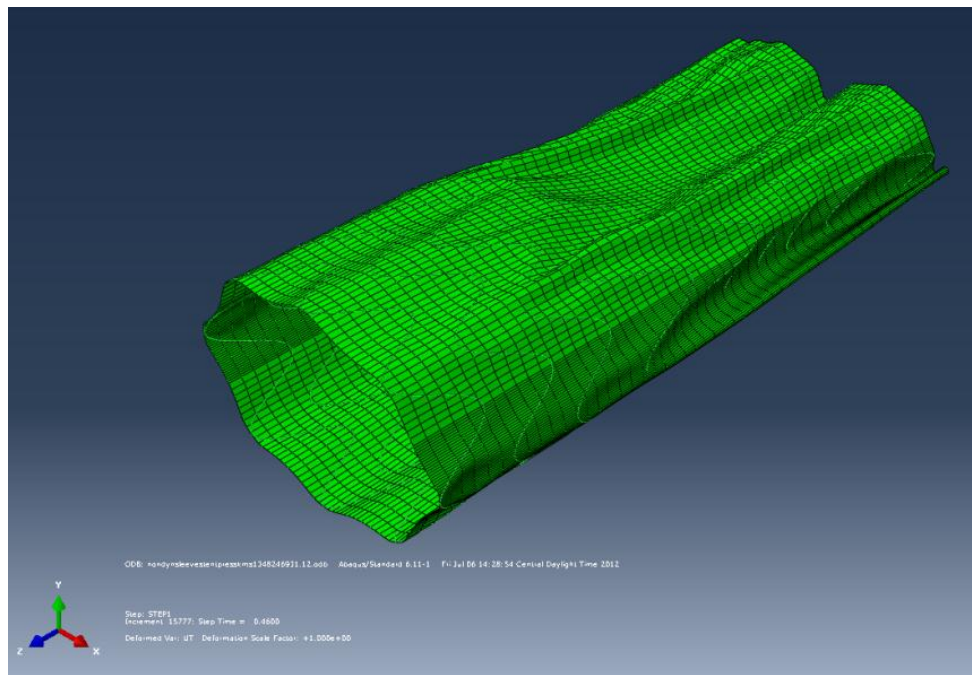
Figure 31: Stent at E=90 GPa compressed by the sleeve under 16.1 mmHg.

compression.

On this same figure is the result of the nonlinear dynamic analysis of the complex stent model. It displays similar results to the experiments where the compression is nonlinear and not concentric. The diameter of the complex model started at 2.55 cm at zero pressure. Equilibrium was achieved through 46% of a set point of 35 mmHg vacuum pressure on the sleeve corresponding to a total converged vacuum pressure of 16.1 mmHg on the stent-sleeve complex. The computational model data follows the average experimental data quite well but as it approaches the pressure of -16.1 mmHg it tapers below the experimental values. This is actually reasonable because the stent does not have the graft material attached. As such with increasing pressure the sleeve is more inclined to compress or dip between the stent wires inducing an error in the integrated area (Figure 32). Figure 31 shows an image of the compressed stent in equilibrium with the sleeve under the final converged pressure of 16.1 mmHg.
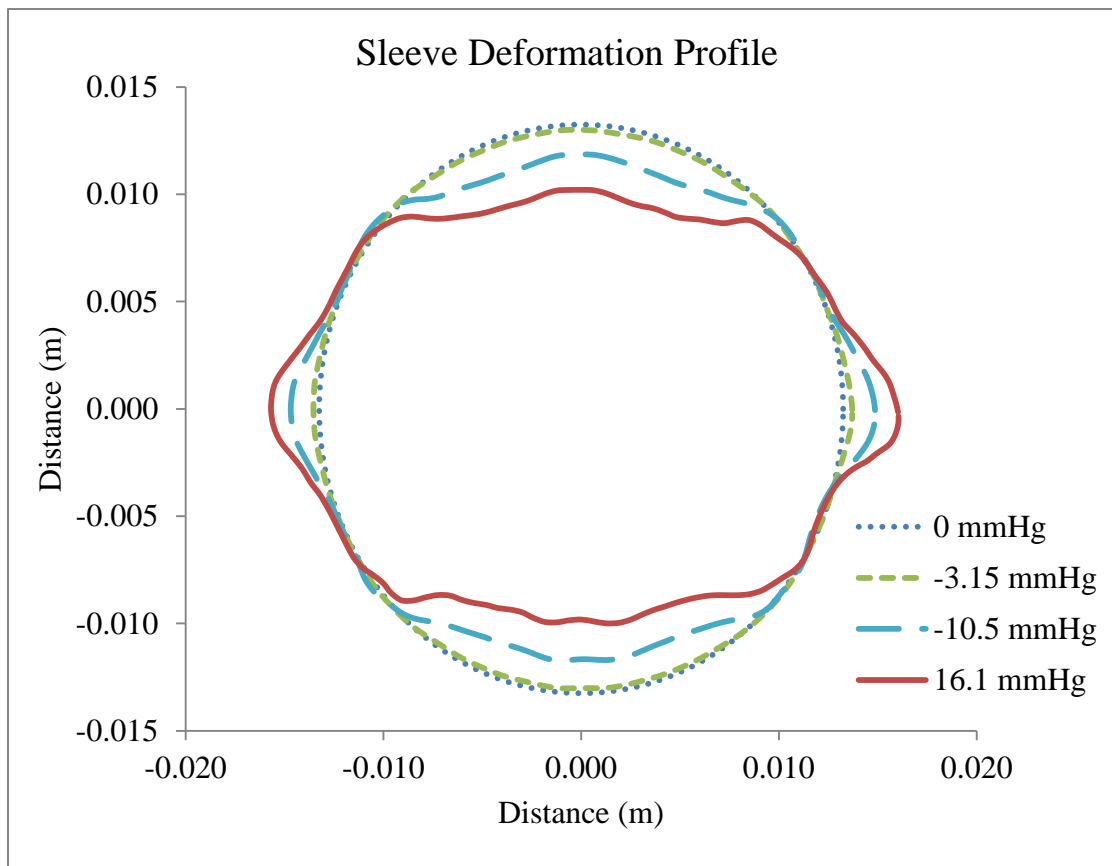
Figure 32: Cross section profile of the sleeve at 1.33 cm from the proximal end while under increasing compression. Note the wavy pattern that that is seen at 16.1 mmHg vacuum as the sleeve dips between stent supports.

CHAPTER 4: DISCUSSION

Endovascular aneurysm repair techniques have provided the opportunity for patients who lack the health for surgical repair a treatment option and selected others a chance to reduce short term morbidity and mortality complications. In order for this to be achieved the stent graft has to be able to undergo large deformations when placed in a catheter. It then must be able to be easily deployed, positioned and radially expand to meet the arterial wall. Once in place it must: maintain its patent lumen, compliantly undergo compression and expansion with the artery under pulsatile blood flow, resist migration, and seal blood from the aneurysm in order to depressurize it. It must do all of this while maintaining good apposition with the aortic wall even in vasculature that may be slightly angulated or contain calcifications. While research has shown these devices to be responsive to oversizing selection in a beneficial manner there is also a known knowledge that too much oversizing is detrimental to SG performance. Longer term studies are showing that the short term benefit of decreased mortality compared to open may be countered with reinterventions and possible device related morbidities. As described, the mechanics that occur at the time of deployment are quite complex and undoubtedly depend on the design and manufacturing of the stent graft to achieve these dynamic results. Additionally, it is likely that the long term fixation characteristics of the stent graft devices are in some manner related to their initial apposition to the arterial wall. This could be derived from their initial deployment and conforming position within the artery.

Currently there is little understanding of the mechanisms and factors involved in the how the device performs in conforming to the aortic vasculature and its nature in the fixation and sealing process during deployment. We consider the ability to capture the compressive nature of the stent graft as something of value in order to improve this understanding and ultimately these devices. Knowing this one can work to build a

computational model and begin to virtually design and investigate varying scenarios inexpensively and quickly in order to optimize the stent design and graft characteristics. Possible factors include wire diameter, amplitude, wavelength, and spacing between coils, and Nitinol transformation temperature as well as graft material, graft taper and leg diameters. Such models can also be utilized to understand how a device will perform within patient specific anatomy and as such allow physicians a better evaluation of the right treatment for each person.

<div align="center">Experimentation</div>

While the experimental setup was conducted in a wooden box there was a level of heat dissipation during experimentation. Typically at the start of an experimental run the heater would need to heat up the air and experimental devices including clamps, optical micrometer sensors, stent grafts, tubing and the wooden box among others. These devices would draw heat from the air, which quickly reached the 99-101°F temperature, into their material. Thus, all materials acted as a heat sink until they too reached more of a consistent temperature close to the set point. Approximately the first 30 minutes of operation had large swings in temperature where the convective heater would turn on and off fairly frequently. Of course each time the front slides were opened to adjust the setup or change devices it would cause a thermal disturbance. Keyence recommends allowing their equipment to stabilize in a temperature for one hour prior to measurements. As well their equipment is calibrated at 68°F and Table A1 in Appendix B shows the readout drift incurred with varying temperatures. The error at 100°F is certainly below our level of interest in the measurements. These temperature variations between when the heater was running and when it was off affected the pressure catheter as well. The transducer was sensitive enough to incur a pressure drift during the five minute experiment interval. To evaluate this effect on the true measurement a dummy experiment was run. The front acrylic door slides were opened as if some changes had to be made introducing a thermal

disturbance. The front doors were then closed and the heater was allowed to oscillate on and off a couple of times while trying to re-establish equilibrium. At this point the process of recording the pressure was initiated but the syringe was not drawn to create a vacuum. Over the five minute interval the variability due to this pressure disturbance was approximately +/- 0.3 mmHg. This variability was not considered significant as the pressure measurements were between 0 and -45 mmHg.

It is worth noting that during the experiments to evaluate the bending properties of the sleeve a large variability in polymer response was noticed based on orientation. While one side would deform under gravitational load to a height of ~24 mm the opposing side, if the sample were flipped over, would deform only ~5 mm. We concluded that while the low density polyethylene polymer may exhibit orientation independent properties we would pursue using the largest value for the bending property. It is likely that the sleeve in fact has a response to loads that incorporates both or all of the orientation dependent properties, depending on direction of the load, but at this point and for simplification we chose to utilize the worst case.

While it seems that the bending properties of the sleeve were the most important to the nature of its deformation the question arises why attain the tensile properties. In fact, the first hypothesis was that the FE model needed the tensile properties in order to deform correctly. When trying this and realizing the model did not perform to expectations the necessary properties were reconsidered. As shown in Figure 33 the tensile results for the polymer sleeve do show a nonlinear behavior at first and then become more linear. As such, a hyper-elastic model could possibly be fit to the average data points for these ten experiments and utilized rather than a linear elastic model. But because the goal was to find the correlation between pressure and diameter the actual material properties of the finite element sleeve only had to mimic the nature of the experimental sleeve. So by decreasing the material thickness until it deformed in a manner representative of the polyethylene essentially the same thing was achieved.
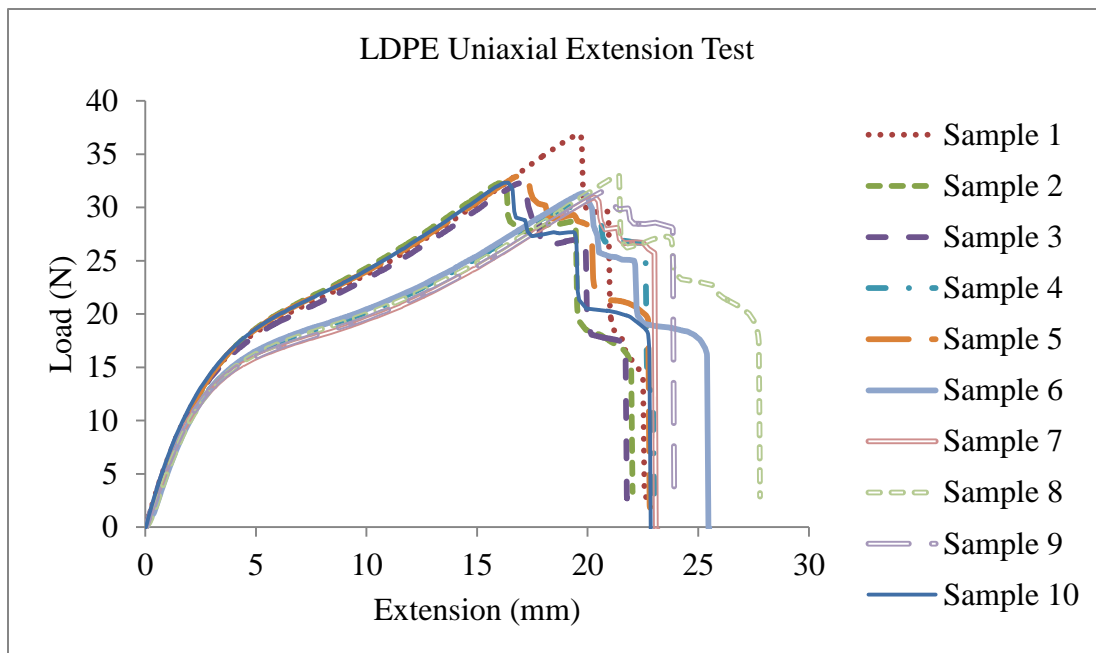
Figure 33: Uniaxial tension tests of LDPE.

Figure 34: Image of Excluder sample that folded when deployed into the
sleeve. The fold is encircled.
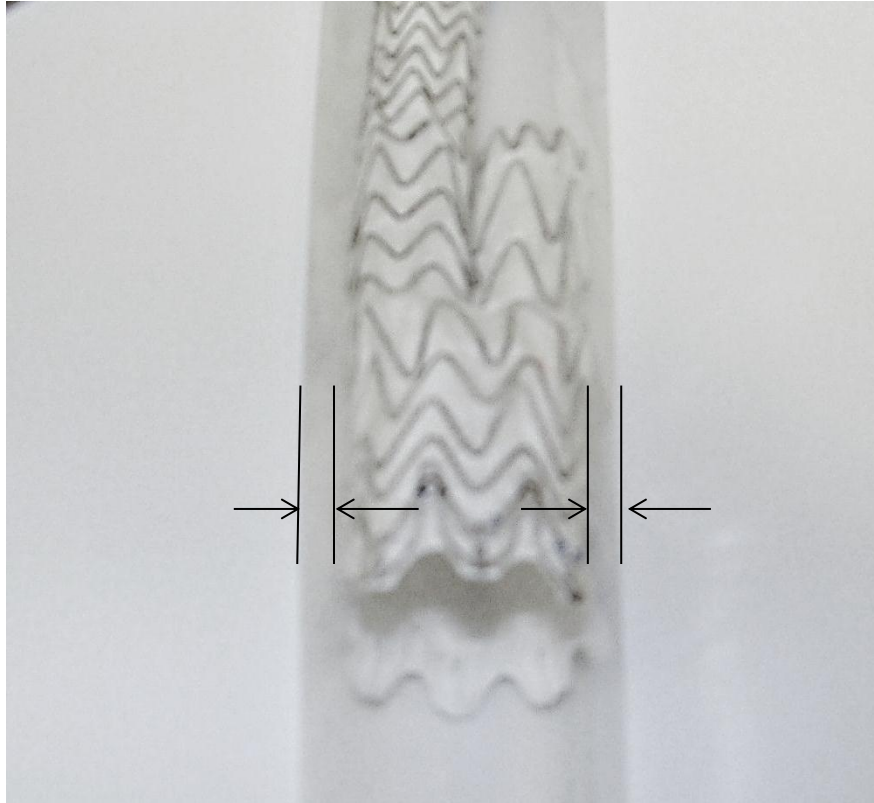
Figure 35: Image showing one of the two devices that was smaller than the sleeve. Arrows display the amount the graft was smaller than the sleeve inducing error in the micrometer measurement. This was the smaller of the two undersized grafts.

The sleeve was a diameter of 1.5 inches laying flat so the circumference was 3 inches and the equivalent max diameter was 2.43 cm. Two of the grafts were slightly larger than the sleeve but by small fractions. One of these was in fact slightly folded when deployed in the sleeve (Figure 34). Similarly, two of the grafts were slightly smaller than the sleeve. In this case the sleeve had the potential to influence the diameter of the graft using the optical micrometer as the sleeve material reflected back its own diameter which was not the diameter of the SG (Figure 35). While these certainly influence the outcome of the experiments we don't feel these occurrences had on overwhelmingly large effect on our data set as the devices were only slightly larger or

smaller than the sleeve and we were looking at the average of across all ten. Additionally the largest influence would be at the lower pressures where higher negative pressure was more inclined to collapse the sleeve against the small grafts. The only caveat would be the single graft where folding occurred. This could have offset the pressure diameter response for this particular graft across the entire loading cycle.

<u>Finite Element Method and Analysis</u>

The displacement driven models attained poor convergence using surface to surface contact. Changing to a node-to-surface based setup resolved the convergence problems and we achieved nearly a 100% convergence with the stent only model and approximately a 75% convergence with the stent graft model. These displacement driven solutions were giving us the nodal contact pressure diameter relationship where the local nodal contact pressures were several factors higher than experiments due to local contact forces (Figure 27). In other words, our general negative vacuum pressure applied to the sleeve can be considered constant across the inner surface of the sleeve. But the contact or interface pressure between the sleeve and graft varies greatly due to overall geometry or shape, local independent deformations, contact interaction, material type and general stent design or architecture. As such, it is difficult to correlate this interface pressure to the experimental vacuum pressure. In fact and as mentioned, if done it would be a rough estimate of the applied vacuum pressure at best. This is why the force equilibrium scenario was chosen. Here pressure was applied to the inner surface of the sleeve and the graft is free to deform under increasing pressure and contact with the sleeve. This in fact provides the correct correlation with our experimental results. The static solution was never achieved in this case and a dynamic quasi-static solution was applied. Abaqus 6.11-1 suggests that geometrically nonlinear static problems that involve buckling or collapse behavior may have several approaches for modeling. One of such ways is to treat these behaviors dynamically by modeling the response with inertial effects included.

Another would be to dampen the system in the static solution scheme but this was not pursued.

Interpretation of Results

Elliptical Compression

Oversizing of a stent graft increases the radial force against the aortic wall. By doing so it increases the frictional force which counteracts distal migration. Naturally, insufficient radial compressive stiffness can result in poor apposition. The anterior view (medial-lateral) experimental orientation shown in Figure 36 shows a compression that is not concentrically symmetric but rather elliptical in nature. This is important when considering the effects of interface pressure due to oversizing on possible device failures such as folding and migration. If this elliptical deformation were the case in-vivo then generally one would expect that the sides that deform along the major axis of the ellipse would also have a higher interface pressure against the arterial wall rather than a more uniform interface pressure had it deformed concentrically. This could influence optimal stent design, barb location, and have an effect on endothelial tissue health where too much pressure could induce possible poor intimal layer ingrowth or localized necrosis.

One of the questions that arise with the fact that all ten grafts collapse elliptically is why. We can speculate to this end that most likely it is a function of the contact interactions of the sleeve with the SG. Particularly is the area of bifurcation and tapering. The Excluder grafts have tendency to be wider, though only slightly where the legs merge with the main stent body on the medial and lateral sides. This is perhaps due to repeated use, the manufacturing process or the fact that the legs themselves are slightly spaced wider than the device body. Also of significance is the distinct taper on the anterior posterior surfaces where the legs also merge with main body. As the sleeve presses against these it can induce an anterior posterior flattening that drives the main

a

b

Figure 36: Anterior view of the Excluder device showing elliptical
            compression.
    (a) Pre-compression
    (b) Fully compressed

body of the stent to follow suit. Appendix C visually shows an explanation of this phenomenon where a portion of the radial force is transferred on the taper to a radial component and an axial component of force. Yet this axial force is resisted by the ~0.75 N of force along the axial sleeve surface or by UZ-boundry constraints in the FE analysis. This helps explain why the sleeve shortens ~1 cm during loading and also why the contact mechanics play such an important role in how the experiments behave. As such one would expect that the stent graft might actually compress in the opposing way as our experiments if no contact is considered, that is in the medial-lateral direction. This can simply be seen in the simplified cross-section in Figure 37 with a uniform negative
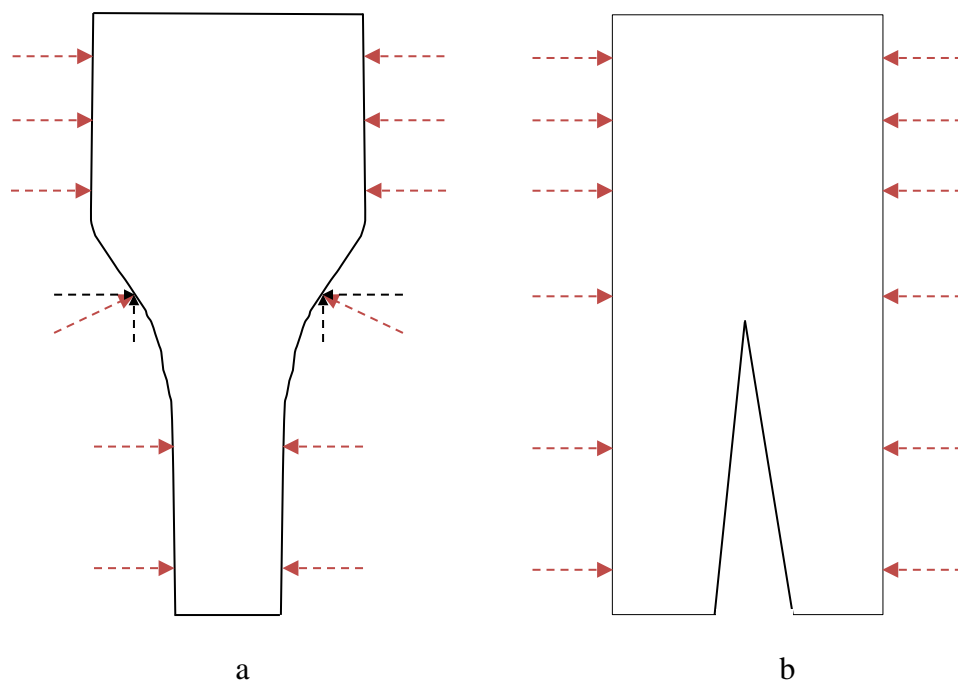

a   b

Figure 37: Loading of SG directly with no sleeve contact considered.
(a) Taper of anterior-posterior reduces radial load and induces an axial component.
(b) Medial-lateral retains the full radial force inducing the most compression in this direction.

pressure load directly on the SG surface. The radial pressure is converted to axial as described above along the taper but now a portion of the radial load is converted to axial reducing its radial force component. With this in consideration the radial load in the orthogonal view of Figure 37b (medial-lateral) is still the initial amount. Certainly stent coil architecture (other than the taper) can play a role and influence how it deforms but those factors would be difficult to ascribe any logical reason to this end from our experimental based evaluations.

From Figure 29 one can note that while the experimental devices under compressive pressure deform elliptically they also on average asymptote to a final compression of approximately 7mm. The graft material is 0.0508 mm (x2) and the stent is 0.3 mm (x2) so one would expect the under the extreme pressure of -50 mmHg the device would certainly be completely collapsed to a diameter of ~0.7 mm. In fact the grafts were complete collapsed during the experiments but this did not always get captured. When imaging the collapsing cross-section (anterior-posterior), in some cases, the sides of the graft did not completely collapse though the center of the graft always did. Additionally, in a couple of scenarios the sleeve-stent graft complex actually slightly rotated. Most likely this rotation was driven by the compression of the stent. It would be unlikely that the sleeve has enough out of plane stiffness to induce such reactive forces that would cause rotation given that that sleeve was always initially set so that no twisting was introduced in the experimental setup. Though small and irregular in occurrence this too would drive the final compressed cross-section higher than expected.

<center>Material Properties and Effect of the Graft</center>

The results of the finite element analysis show that a linear elastic modulus for the stent at 90 GPa matches well for up to the converged 16 mmHg.). Vad et al. [31] provided data from literature for a modulus of 40 GPa. The discrepancy may be explained by considering that the Excluder Nitinol material may have different designated properties
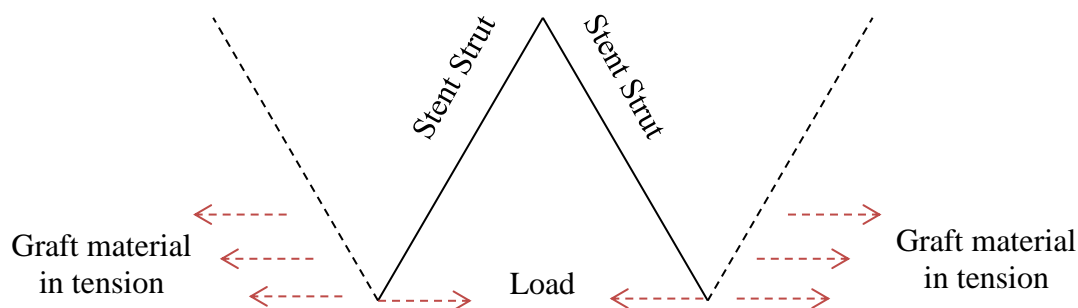
Figure 38: Effect of the graft material where a single stent under compression pulls on the adjacent graft material distributing the load to nearby stents.

or composition than those used in their work. Additionally one must take into account that our model is only derived from the stent wire geometry and neglects the graft fabric. One could argue the lack of the grafts necessity due to the fabric like material having no effect on the compressive nature of the graft as it typically just folds over itself and the stent under an inwardly driven load. Yet as we have learned the graft material plays a critical role in the function of the stent graft device outside of being just a conduit for blood flow in order to depressurize the aneurysm. In fact and most certainly for open cell based stent grafts the graft material acts as the in-plane axial and circumferential support for the stent. It is the analog to the exterior sheeting put on a modern stick frame house. The house will stand on its own but the sheeting ties all the framing timber together and a load on one side gets distributed among the other sides of the house supports. Similarly, when you begin to compress the stent as a whole it causes two different load conditions. In each the graft interacts with the stent and helps to distribute the load. First is the fact that under radial compression a single stent 'v' strut will slightly collapse. If the bottom of the 'v' stent collapses it transfers this load through the graft material to neighboring stents and pulls on them to help carry the load as well (meaning the graft carries and transmits tensile force) (Figure 38). The second observation of the role of the graft is

similarly related to this property. Under the circumstance of asymmetric radial compression where localized loading occurs and the interface pressure is not uniform (nearly instantly) it begins to twist stent segments. Again looking at a single 'v' stent (Figure 39) if you shear the stent so that the legs are no longer in the same plane but offset from each other by a distance 'd' then you begin to see a tensile load on the graft material between one leg and the other. This load is also transmitted to adjoining stents in the circumferential direction and along the z-axis in this case pulling the stent coil above or below the stent segment under the sheared deformation. These two examples layout the importance of the graft material to the structural integrity of the device and its ability to resist deformation. When considering the reasoning of why the modulus was nearly two times higher than that reported in other studies this too should be in the consideration. A stent only model has to be able to account for the fact that a local radial
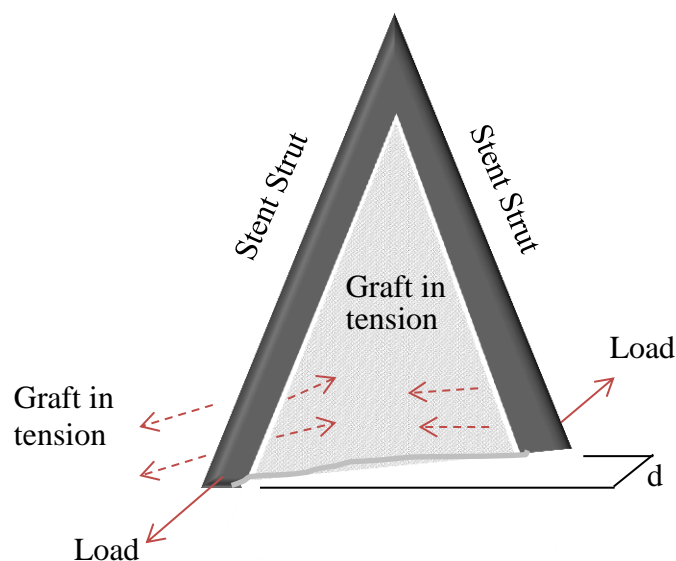

Figure 39: Stent segment under local torsion inducing tension in the graft material which distributes the load to other local stent segments.

load in a stent graft is actually carried by more than one stent segment and more than one coil via the graft interactions. If a model like ours does not include the graft material then using a stent with a higher stiffness is a conceivable resolve to account for this. Another approach could have been to keep the modulus at the reported modulus (40 GPa) and increase the diameter of the stent.

Hysteresis

The experiments resulted in test data that exhibits hysteresis during the load-unload cycle. This response was likely caused by a loss of energy from friction between the graft and the polymer tubing. It is also possible that some energy was lost during the cycle to friction between the graft and the stent. This is considered because the contact interface between the graft and stent is imperfect. Though they are attached by adhesive in the case of the Excluder or sewn together on other devices there is still an opportunity for one surface to slightly slide along the other, though it may be small. A similar effect of the captured hysteresis is conceivable in-vivo, but remains to be verified.

Related Works

Limited publications have been established and to our knowledge few research groups have investigated the pressure diameter relationship of these medical devices and those that are have used different approaches. While literature contains FE analysis of arterial stents we have found few publications where the FEM accounts for bifurcated AAA stent grafts. It seems, to some degree, these pursuits have been left up to the individual manufacturers. Yet, academic investigation can additionally be useful in not only helping understanding the mechanics involved but also in achieving consistent testing standards (computational and bench top) even between manufacturers for benchmarking.

In 2000 a publication by Duda et. al. [9] investigated the mechanical properties of endovascular stents. They tested two related scenarios; the hoop strength for balloon

expandable stents and the chronic outward force or radial resistive force for self-expanding stents. In their study they inserted balloon expanded stents in compliant tubing which was placed in an airtight chamber. Positive pressure was forced in the air chamber which applied a negative pressure on the stent to collapse it. This setup was placed in cabinet at $37^{o}C$ +/- $2^{o}C$. As they define it this hoop strength test assesses the pressure required to collapse a stent that has been expanded to the rated burst pressure of the balloon. Their chronic outward force on the other hand is considered a measure of the force the stent exerts on the artery as it tries to expand to its nominal diameter with the vessel is relaxed. This is similar to what we have been considering the interface pressure. To capture this they wrapped a piece of thin mylar film around the stent. One end was attached to a fixed based and then wrapped around the stent. Then the other end was circled around a roller in close proximity to the fixed base and continued vertically finally attaching to a MTS machine. A vertical force by the MTS was then redirected to a circumferential compression of the stent. These experimental setups are similar to ours. They too have challenges and as discussed may not allow the device to freely deform based on stent wire design and properties. As discussed in the hoop strength test the compliant tube may attenuate nonuniform deformation. In the chronic outward force you may get uneven loading due to friction and local impingement where the roller and base meet the stent and Mylar construct. Their work does to some degree resemble similar attempts using only stents as our work with stent grafts, though the end goals differ at this stage.

In 2008 Kleinstreuer et al. [17] performed a finite element study of tubular diamond-shaped stent grafts. This was completed using two Nitinol materials commonly used in industry and two graft materials as well (PET and ePTFE). The effects of three scenarios were considered on the stent-graft loading and fatigue life; crimping of the SG into the catheter, deployment and cyclic pressure loading of the main device body. Though the study was not looking at the pressure-diameter relationship but rather the effects of

loading on strain and on fatigue they did capture some insightful data that can be related to our work. They analyzed a cylindrical closed cell diamond patterned stent and did not include any graft material for the crimping and deployment scenarios. During crimping the graft sheath is folded and thus they did not included its effects. Also, circumferential symmetry was enforced and the stent was fixed in the axial direction at the end nodes during crimping. Here zero contact friction was utilized and a penalty interaction property was used. In the deployment (sealing loading) scenario it was assumed that the artery wall prevent the stent graft from completely expanding implying the stent to be under compression and the graft material did not encountering significant tensile stress. Therefore they did not include the graft material. A contact friction factor of 0.25 was included to prevent slipping and a uniform pressure was imputed on the inner artery wall. Displacement boundary conditions were the same as that for the crimping. Our work included a combination of these approaches. While we used a sleeve it acted something like a crimping force but not concentrically symmetric as we allowed the sleeve-stent complex to freely deform at will which a crimper does not. This crimping action occurred similar to our displacement driven solution scheme but we eventually moved on to the force equilibrium which was similar to the deployment scenario used in their study. From their study they attained a radial crimping force versus stent OD curve shown in Figure 40. As noted in their paper commercial stent-graft design refers to the traditional notation of 'circumferential' forces/stress/strains as 'radial' forces/stresses/strains. As such I'll use their convention in this section of the discussion to be consistent. You can clearly see a point for both stent materials where the slope of radial force resistance significantly decreases. For NITI-2 this point is near a diameter of 25 mm or a 16% decrease in diameter. This means the initial radial force resistance is strong and for a given increase in force the stent graft linearly matches this force with resistance. Once you get beyond this 16% point an equal increase in force is met with a smaller increment in force resistance making it easier to compress or largely deform the stent graft. While
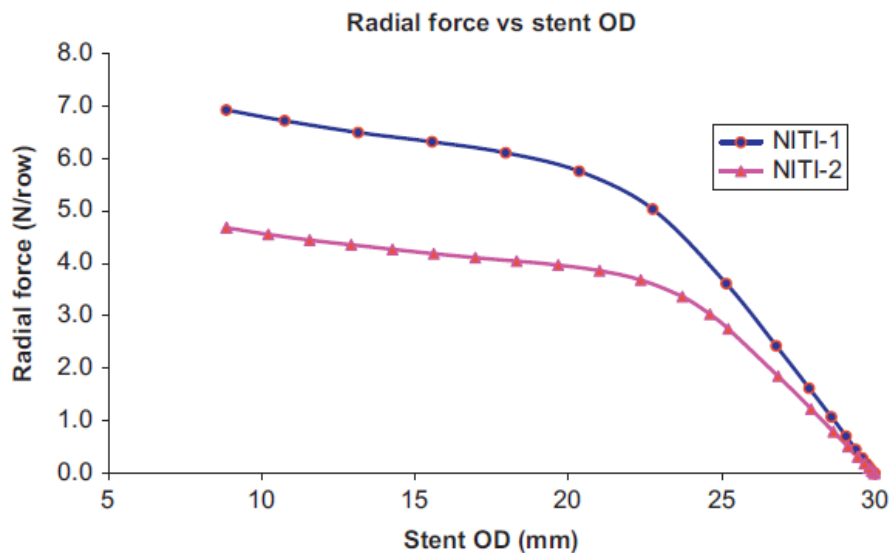
Figure 40: Relationship between the radial force and the stent diameter.

Reproduced from "Computational mechanics of Nitinol stent grafts[17]" with permission from Dr. Kleinstreuer (North Carolina State University).

this drop in slope occurs at a ~16-23 % change in diameter from their data (depending on Nitinol material) our data shows it occurring at a ~6% change in diameter. This can be resolved by considering the effect of a closed cell diamond shaped stent compared to our open cell sinusoidal stent. Certainly their stent has more metal that is symmetrically placed to resist radial deformation. Additional considerations may be that the Excluder's Nitinol material may be different than what they used in their analysis or that our devices have undergone more experiments causing fatigue and the devices to deform sooner. It is important to note that our model is not cylindrical but bifurcated and has non-uniform sinusoidal stent paths that are free to deform unsymmetrically.

As discussed by Stoeckel et al. [30] the phenomena in the previous study and ours are typical of Nitinol. As most engineering materials exhibit a linear stress-strain relationship for loading and unloading, Nitinol is different. Nitinol when exposed to an

initial stress will strain, and then subsequent larger strains can be achieved with smaller stress increments. This is considered the loading plateau and is reached at approximately 8% strain. One of the questions undetermined is how much of this plateau drives the compressive properties of the SG and how much is a function of its geometric design in our experiments. Because we used linear elastic material properties for the stent in our model and matched the experiments well through a pressure of -16 mmHg, it would lead one to believe the geometry may play a large role. The wire strain would have to be investigated to confirm this hypothesis.

Limitations

This work is certainly not without its limitations. The most obvious is that the model at this point is primarily simulated as a stent only which does not include the graft material and its effects on the device mechanics. While a stent graft model as discussed is in the works it is not yet finished. The fact that this is a stent only model one can see that the finite element boundary constraints that are placed on the graft leads to its use in primarily 'idealized' tubular shaped aneurysms. This is due to the fact that the medial-lateral sides of the device are constrained in the anterior-posterior directions in order to act as a proctor for the graft material, which in turn restricts the models freedom to conform to highly angulated vasculature.

The model does not account for friction between the graft and sleeve. Friction certainly is a part of the experimental dynamics and certainly it plays a role in-vivo. The friction between the graft and stent are of less concern. For example, while they may locally translate or rotate relative to one another they may do so only on a fractionally small scale compared to the device and the sleeve as a whole.

The experimental setup uses two loading-unloading cycles in order to attain the pressure-diameter relationship. While the initial pressure and diameters were used in each case and a normalized percent change in equivalent diameters were calculated this

still does not resolve the fact that the diameter of one device orientation was independently captured from the orthogonal orientation. This could lead to error in the diameter measurements as the first loading cycle could induce a biased propensity of the device to deform the same in the loading and unloading cycle in the ensuing orthogonal orientation.

<div align="center">Future Directions</div>

Two other groups (BioMMeda lab at the University of Ghent and Zarins Lab at Stanford University) have worked in a similar fashion as we have to begin to understand the mechanics the endovascular graft undergoes during crimp, deployment and conforming process post deployment with the artery wall. They focus on working to understand the mechanics leading to SG apposition and effects of possible migration that may lead to long term durability. Though it is not primarily focused on building a detailed model that mimics the dynamics of the graft in experimentation it is worth noting. We can certainly see this as a possible future pursuit as we consider applying our models to understand similar scenarios and more clinically related problems.

The BioMMeda research group from the University of Ghent, Belgium have undertaken related research to understand the dynamical behavior of endovascular grafts in patient specific anatomy. In a publication by De Bock et al.[2] the group creates a 3D model of patient specific aneurysm anatomy taken from CT images. A 3D model of endovascular grafts are also constructed from CT images as well. Then the SGs are compressed using displacement boundary conditions and positioned along the centerline of the patients anatomy. The crimping load on the stent grafts is then removed and the device is allowed to expand and conform to the vasculature. The method allows simulations to predict the device conformation of a SG to the patient specific vasculature.

Similarly the Zarins Lab at Stanford is working along a similar pursuit to resolve a FE modeling approach for evaluating the risk of endovascular graft migration. From an

abstract at the 2011ASME 6th Frontiers Biomedical Device Conference[23] they used three representative patient abdominal aneurysm models with varying aortic tortuosity and decreased proximal neck length. They are using a simplified stent graft model with a single cylindrical tube for the graft and with z-based stents on the inside of the graft. With the incorporation of fluid flow and representative pulsatile forces they coupled their mechanical based analysis, including friction, with the fluid dynamics. Their simulation approach induces a pre-stress in the artery to represent the in-vivo mean arterial pressure load.

Though the research here is not focused on modeling methodology or clinical relevance it is the foundation for such work. And, though we cycled our devices though complete compression-decompression to get the dynamics of the graft, undoubtedly, one can resolve that in-vivo the graft would never collapse until complete occlusion unless a material failure occured. It may be that in equilibrium with the artery the device displays a non-concentric based deformed shape, possibly an elliptical one. Yet the ability to tie our experimental or modeled data of a pressure induced compression to the interface pressure of the stent graft is difficult. At best, one may only draw an estimated amount of interface pressure at the low end of the device compression from our data. This is because the oversizing selection of devices is based on circular cross-sections while our data is elliptical in nature and was mathematically mapped back to the equivalent circular diameter.

Yet, the pursuit of this work was to formulate an experimental methodology that captured the radial compressive behavior of endovascular devices. We then set out to leverage our ability to attain that data and build a computational stent based model whose geometry was realistic and whose dynamics approximate the average compressive nature of the device. Our results suggest that the developed model is representative of our experiments and the model may be used to interrogate how a SG will perform during

certain stages of deployment and immediately after deployment in vivo, with some caution in regard to the stated limitations.

APPENDIX A

SYNTAX FOR THE FIRST COIL

COIL = 1

t = 0

*DO,j,1,127

    K,,Radius*cos(t), Radius*sin(t), (C1HEIGHT)*t + C1AMPA*sin(t*PEAKS) -

    (C1SPACING)

t = t – dt

*ENDDO

APPENDIX B

KEYENCE LS-7070M DATA TABLE

Table A1: Drift properties versus temperature for the Keyence LS-7070M optical
micrometer.

Temperature	0°C (32°F)	10°C (50°F)	20°C (68°F)	30°C (86°F)	40°C (104°F)	50°C (122°F)
Drift (μm)	+1.8	+0.8	0	-0.8	-1.8	-3.0

APPENDIX C

ELLIPTICAL COMPRESSION OF THE EXCLUDER EVG

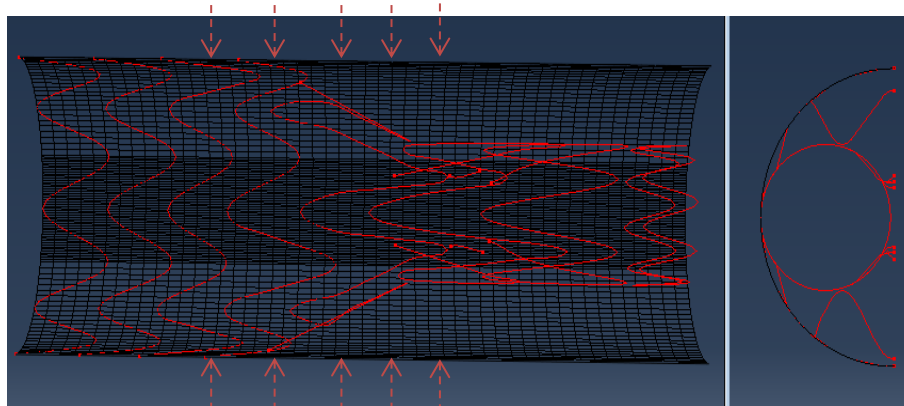Figure C1: Initial state of the stent sleeve complex. Dashed arrows
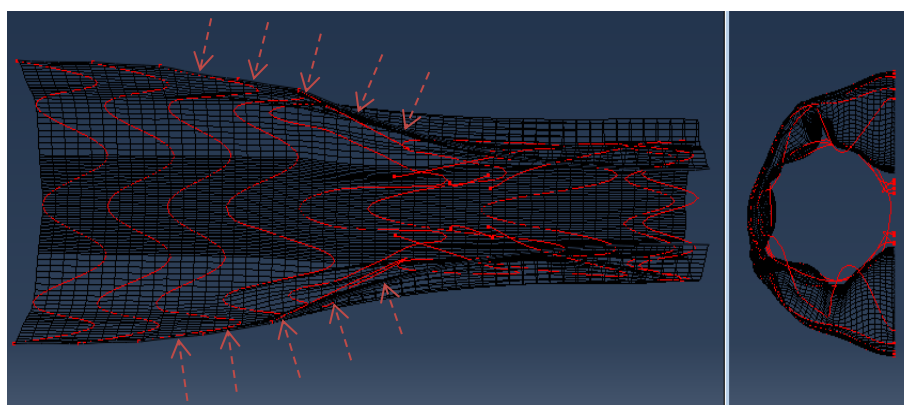show applied pressure direction.

Figure C2: Image of stent under compression with a pressure of -8.05
mmHg. This displays how the sleeve conforms to the stent
at the taper.
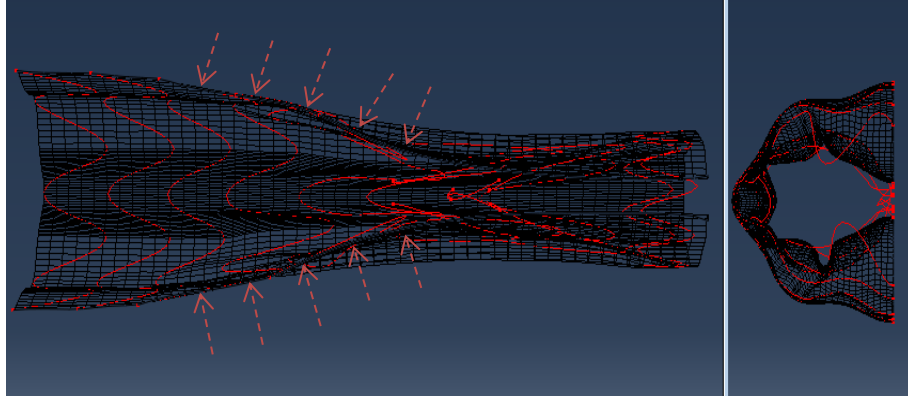
Figure C3: Compression of stent at -16.1mmHg. Note how the
          normal force through the taper has radial and axial force
          components.

REFERENCES

1. Albuquerque, F. C., B. H. Tonnessen, R. E. Noll, G. Cires, J. K. Kim, and W. C. Sternbergh. Paradigm shifts in the treatment of abdominal aortic aneurysm: trends in 721 patients between 1996 and 2008. *Journal of vascular surgery* 51:1348–52; discussion 1352–3, 2010.

2. De Bock, S., F. Iannaccone, G. De Santis, M. De Beule, D. Van Loo, D. Devos, F. Vermassen, P. Segers, and B. Verhegghe. Virtual evaluation of stent graft deployment: A validated modeling and simulation study. *Journal of the mechanical behavior of biomedical materials* 13C:129–139, 2012.

3. Brewster, D. C., J. L. Cronenwett, J. W. Hallett, K. W. Johnston, W. C. Krupski, and J. S. Matsumura. Guidelines for the treatment of abdominal aortic aneurysms. Report of a subcommittee of the Joint Council of the American Association for Vascular Surgery and Society for Vascular Surgery. *Journal of vascular surgery* 37:1106–17, 2003.

4. De Bruin, J. L., A. F. Baas, J. Buth, M. Prinssen, E. L. G. Verhoeven, P. W. M. Cuypers, M. R. H. M. van Sambeek, R. Balm, D. E. Grobbee, and J. D. Blankensteijn. Long-term outcome of open or endovascular repair of abdominal aortic aneurysm. *The New England journal of medicine* 362:1881–9, 2010.

5. Chadi, S. a, B. W. Rowe, K. N. Vogt, T. V. Novick, J. R. Harris, G. Derose, and T. L. Forbes. Trends in management of abdominal aortic aneurysms. *Journal of vascular surgery* 55:924–8, 2012.

6. Chaikof, E. L., J. D. Blankensteijn, P. L. Harris, G. H. White, C. K. Zarins, V. M. Bernhard, J. S. Matsumura, J. May, F. J. Veith, M. F. Fillinger, R. B. Rutherford, and K. C. Kent. Reporting standards for endovascular aortic aneurysm repair. *Journal of Vascular Surgery* 35:1048–1060, 2002.

7. Crawford, E. S., S. a Saleh, J. W. Babb, D. H. Glaeser, P. S. Vaccaro, and a Silvers. Infrarenal abdominal aortic aneurysm: factors influencing survival after operation performed over a 25-year period. *Annals of surgery* 193:699–709, 1981.

8. Dattilo, J. B., D. C. Brewster, C.-M. Fan, S. C. Geller, R. P. Cambria, G. M. LaMuraglia, A. J. Greenfield, S. R. Lauterbach, and W. M. Abbott. Clinical failures of endovascular abdominal aortic aneurysm repair: Incidence, causes, and management. *Journal of Vascular Surgery* 35:1137–1144, 2002.

9. Duda, S. H., J. Wiskirchen, G. Tepe, M. Bitzer, T. W. Kaulich, D. Stoeckel, and C. D. Claussen. Physical properties of endovascular stents: an experimental comparison. *Journal of vascular and interventional radiology : JVIR* 11:645–54, 2000.

10. Ernst, C. B. Abdominal aortic aneurysm. *The New England journal of medicine* 328:1167–72, 1993.

11. Forsdahl, S. H., K. Singh, S. Solberg, and B. K. Jacobsen. Risk factors for abdominal aortic aneurysms: a 7-year prospective study: the Tromsø Study, 1994-2001. *Circulation* 119:2202–8, 2009.

12. Hallett, J. W., D. M. Marshall, T. M. Petterson, D. T. Gray, T. C. Bower, K. J. Cherry, P. Gloviczki, and P. C. Pairolero. Graft-related complications after abdominal aortic aneurysm repair: reassurance from a 36-year population-based experience. *Journal of vascular surgery* 25:277–84; discussion 285–6, 1997.

13. Hölzenbein, T. J., G. Kretschmer, S. Thurnher, M. Schoder, E. Aslim, J. Lammer, and P. Polterauer. Midterm durability of abdominal aortic aneurysm endograft repair: A word of caution. *Journal of Vascular Surgery* 33:46–54, 2001.

14. Johnston, K. W., R. B. Rutherford, M. D. Tilson, D. M. Shah, L. Hollier, and J. C. Stanley. Suggested standards for reporting on arterial aneurysms. , 1991.

15. Katzen, B. T., and A. a MacLean. Complications of endovascular repair of abdominal aortic aneurysms: a review. *Cardiovascular and interventional radiology* 29:935–46, 2006.

16. Kazmers, A., L. Jacobs, A. Perkins, S. M. Lindenauer, and E. Bates. Abdominal aortic aneurysm repair in Veterans Affairs medical centers. *Journal of Vascular Surgery* 23:191–200, 1996.

17. Kleinstreuer, C., Z. Li, C. a Basciano, S. Seelecke, and M. a Farber. Computational mechanics of Nitinol stent grafts. *Journal of biomechanics* 41:2370–8, 2008.

18. Kratzberg, J. a, J. Golzarian, and M. L. Raghavan. Role of graft oversizing in the fixation strength of barbed endovascular grafts. *Journal of vascular surgery* 49:1543–53, 2009.

19. Lawrence, P. F., C. Gazak, L. Bhirangi, B. Jones, K. Bhirangi, G. Oderich, and G. Treiman. The epidemiology of surgically repaired aneurysms in the United States. *Journal of vascular surgery* 30:632–40, 1999.

20. Liakishev, a a. [Comparison of Endovascular Aneurysm Repair With Open Repair in Patients With Abdominal Aortic Aneurysm, 30-day Operative Mortality RESULTS: Randomised Controlled Trial. Results of the EVAR 1 Trial.]. *Kardiologiia* 44:90, 2004.

21. Mohan, I. V., R. J. Laheij, and P. L. Harris. Risk factors for endoleak and the evidence for stent-graft oversizing in patients undergoing endovascular aneurysm repair. *European journal of vascular and endovascular surgery : the official journal of the European Society for Vascular Surgery* 21:344–9, 2001.

22.   Parodi, J. C., J. C. Palmaz, H. D. Barone, and B. Aires. Original articles Transfemoral Intraluminal Graft Implantation for Abdominal Aortic Aneurysms. 491–499.

23.   Prasad, A., C. K. Zarins, and C. A. Figueroa. BioMed2011-66022 A FINITE ELEMENT APPROACH FOR EVALUATING THE RISK OF ENDOGRAFT. , 2011.

24.   Prinssen, M., E. L. G. Verhoeven, J. Buth, P. W. M. Cuypers, M. R. H. M. van Sambeek, R. Balm, E. Buskens, D. E. Grobbee, and J. D. Blankensteijn. A Randomized Trial Comparing Conventional and Endovascular Repair of Abdominal Aortic Aneurysms. *New England Journal of Medicine* 351:1607–1618, 2004.

25.   Resch, T., M. Malina, B. Lindblad, J. Malina, J. Brunkwall, and K. Ivancev. The impact of stent design on proximal stent-graft fixation in the abdominal aorta: an experimental study. *European journal of vascular and endovascular surgery : the official journal of the European Society for Vascular Surgery* 20:190–5, 2000.

26.   Rutherford, R. B., and W. C. Krupski. Current status of open versus endovascular stent-graft repair of abdominal aortic aneurysm. *Journal of vascular surgery* 39:1129–39, 2004.

27.   Schanzer, a., and L. Messina. Two Decades of Endovascular Abdominal Aortic Aneurysm Repair: Enormous Progress With Serious Lessons Learned. *Journal of the American Heart Association* 1:e000075–e000075, 2012.

28.   Schumacher, H., H. H. Eckstein, F. Kallinowski, and J. R. Allenberg. Morphometry and Classification in Abdominal Aortic Aneurysms: Patient Selection for Endovascular and Open Surgery. *Journal of Endovascular Surgery* 4:39–44, 1997.

29.   Sternbergh, W. C., P. J. Nordness, J. W. York, M. S. Conners, G. Carter, and S. R. Money. Endo-exuberance to endo-reality: trends in the management of 431 AAA repairs between 1996 and 2002. *Journal of endovascular therapy : an official journal of the International Society of Endovascular Specialists* 10:418–23, 2003.

30.   Stoeckel, D., A. Pelton, and T. Duerig. Self-expanding nitinol stents: material and design considerations. *European radiology* 14:292–301, 2004.

31.   Vad, S., A. Eskinazi, T. Corbett, T. McGloughlin, and J. P. Vande Geest. Determination of coefficient of friction for self-expanding stent-grafts. *Journal of biomechanical engineering* 132:121007, 2010.

32.   Vorp, D. A. Personal communication during lab tours, Iowa City, IA. , 2011.

33. Wald, M. J., J. M. Considine, K. T. Turner, and U. S. F. Service. Measuring the Elastic Modulus of Soft Thin Films on Substrates Dept . of Mechanical Engineering , University of Wisconsin , Madison , WI. 0–7, 2010.

34. Wanhainen, A., D. Bergqvist, K. Boman, T. K. Nilsson, J. Rutegård, and M. Björck. Risk factors associated with abdominal aortic aneurysm: a population-based study with historical and current data. *Journal of vascular surgery* 41:390–6, 2005.

35. Zarins, C. K., D. a Bloch, T. Crabtree, A. H. Matsumoto, R. a White, and T. J. Fogarty. Stent graft migration after endovascular aneurysm repair: importance of proximal fixation. *Journal of Vascular Surgery* 38:1264–1272, 2003.